Widespread Increase in Enhancer—Promoter Interactions during Developmental Enhancer Activation in Mammals

Zhuoxin Chen[1], Valentina Snetkova[2], Grace Bower[1], Sandra Jacinto[1], Benjamin Clock[1], Iros Barozzi[2,†,], Brandon J. Mannion[2], Ana Alcaina-Caro[3], Javier Lopez-Rios[3], Diane E. Dickel[2,†], Axel Visel[2,4,5,6], Len A. Pennacchio[2,4,5,6] and Evgeny Z. Kvon[1,*]

[1] Department of Developmental & Cell Biology, School of the Biological Sciences, University of California, Irvine, CA, USA;

[2] Environmental Genomics and Systems Biology Division, Lawrence Berkeley National Laboratory, Berkeley, CA, USA;

[3] Centro Andaluz de Biología del Desarrollo, CSIC/JA/Universidad Pablo de Olavide, Seville, 41013, Spain;

[4] U.S. Department of Energy Joint Genome Institute, Walnut Creek, CA, USA;

[5] School of Natural Sciences, University of California, Merced, CA, USA;

[6] Comparative Biochemistry Program, University of California, Berkeley, CA, USA

[†] Present address: Center for Cancer Research, Medical University of Vienna, Vienna, Austria (I.B.); Octant, Inc, Emeryville, CA 94608, USA (D.E.D)

* Correspondence should be addressed to EKvon@uci.edu

Abstract

Remote enhancers are thought to interact with their target promoters via physical proximity, yet the importance of this proximity for enhancer function remains unclear. Although some enhancer–promoter loops are cell-type-specific, others are stable across tissues or even display reduced physical proximity upon activation. A major challenge is that relatively few enhancers are functionally characterized *in vivo,* making it difficult to draw generalized conclusions about enhancer–promoter looping during developmental gene activation. Here, we investigate the 3D conformation of enhancers during mammalian development by generating high-resolution tissue-resolved contact maps for nearly a thousand mammalian enhancers with known *in vivo* activities in ten murine embryonic tissues. We performed enhancer knockouts in mice, which validated newly identified enhancer–promoter chromatin interactions. The majority of enhancers display tissue-specific 3D conformations, and both enhancer–promoter and enhancer–enhancer interactions are significantly stronger upon enhancer activation *in vivo*. Less than 14% of enhancer–promoter interactions form stably across tissues; however, corresponding enhancers still display highly-tissue-specific activities indicating that their activity is uncoupled from a chromatin interaction with promoters. We find that these invariant interactions form in the absence of the enhancer and are mediated by adjacent CTCF binding. We also identified putative *in vivo* target genes for enhancers linked to congenital malformations, neurodevelopmental disorders, and autism, demonstrating the utility of our dataset for understanding human congenital disorders. Our results highlight the general significance of enhancer–promoter physical proximity for developmental gene activation in mammals.

Introduction

Enhancers, or *cis*-regulatory elements, ensure precise spatiotemporal control of gene expression during development. This process is mediated by transcription factors (TFs) and co-activators, which relay regulatory information from enhancers to their target promoters (Serebreni and Stark 2021; Shlyueva, Stampfel, and Stark 2014; Long, Prescott, and Wysocka 2016; Visel, Rubin, and Pennacchio 2009; Kvon et al. 2021), across distances that can sometimes exceed one megabase (Lettice et al. 2002; Long et al. 2020; Padhi et al. 2021; Yanchus et al. 2022). This enhancer–promoter (E–P) communication is thought to occur within so-called topologically associated domains (TADs), fundamental organizational units of the genome formed through the process of loop extrusion by cohesin and CCCTC-Binding Factor (CTCF; (Robson, Ringel, and Mundlos 2019; Schoenfelder and Fraser 2019a; Dixon et al. 2012; Nora et al. 2012; Rao et al. 2014). Disruption of TADs or intra-TAD chromatin interactions causes erroneous downregulation of gene expression or gene activation and can lead to human disease, indicating the importance of proper E–P communication for gene activation (Ibn-Salem et al. 2014; Lupiáñez et al. 2015; Franke et al. 2016; Bhatia et al. 2013; Uslu et al. 2014; Lettice et al. 2011; Northcott et al. 2014).

Remote enhancers are thought to communicate with their target genes via physical proximity established by chromatin looping (Tolhuis et al. 2002; Bulger and Groudine

1999; Schoenfelder and Fraser 2019b; Furlong and Levine 2018; Shlyueva, Stampfel, and Stark 2014; Long, Prescott, and Wysocka 2016; Robson, Ringel, and Mundlos 2019; Oudelaar and Higgs 2021). However, whether physical proximity is linked to enhancer function remains unclear. One model suggests that E–P contacts are formed only during gene activation. Indeed, the establishment of E–P interactions at many genetic loci occurs coordinately with gene transcription (Javierre et al. 2016; Andrey et al. 2013; Tolhuis et al. 2002; Montavon et al. 2011; Siersbæk et al. 2017; Madsen et al. 2020; Freire-Pritchett et al. 2017; Rubin et al. 2017). In line with this, artificial tethering of an enhancer to the developmentally silenced β-globin promoter results in an ectopic gene activation (Deng et al. 2012, 2014; Morgan et al. 2017), suggesting a potentially instructive role of chromatin looping in E–P communication and gene activation. An alternative model is that E–P contacts are stable and/or pre-formed by higher-order chromatin organization, and thus not temporally linked to gene activation. In support of this model, many E–P chromatin interactions do not correlate with target gene transcription. For example, mouse limb enhancers at the *HoxD* and *Shh* loci, human fibroblast and keratinocyte enhancers, and many early *Drosophila* enhancers appear to form E–P chromatin loops even when the genes are not expressed (Ghavi-Helm et al. 2014; Andrey et al. 2017; Simmons et al. 2021; Rubin et al. 2017; Espinola et al. 2021; Jin et al. 2013; Montavon et al. 2011; Lonfat et al. 2014). In a third model, gene activation is accompanied by reduced physical E–P proximity. For example, *Sonic hedgehog* (*Shh*) and *Sox2* enhancers that are active during

differentiation of mouse embryonic stem cells into neuronal progenitors can activate gene transcription even in the absence of increased E–P physical proximity, challenging a simple looping model (Alexander et al. 2019; Benabdallah et al. 2019). While all these models exist in principle, the predominant mode of activation for developmental tissue-specific enhancers remains unclear since past research has focused on well-studied genetic loci. Another challenge is that relatively few enhancers are functionally characterized *in vivo* (Kvon 2015; Mannion et al. 2022; Pennacchio et al. 2006) making it challenging to separate E–P interactions linked to specific gene activation from other types of chromatin interactions.

To better understand E–P interactions during mammalian development, we utilized a unique resource of experimentally verified human and mouse enhancers (Visel et al. 2006; Pennacchio et al. 2006). Many of these enhancers have been shown to be critical for developmental and disease processes (Snetkova et al. 2021; Attanasio et al. 2013; Dickel et al. 2016, 2018; Fakhouri et al. 2014; Kragesteen et al. 2018; Kvon et al. 2016, 2020; Lupiáñez et al. 2015; Osterwalder et al. 2018; Pattabiraman et al. 2014; Visel et al. 2010). However, the 3D nuclear organization of these loci remains largely uncharacterized. We thus generated high-resolution enhancer interactome maps across 10 mouse embryonic tissues for 935 *bona fide* developmental enhancers with characterized *in vivo* activity at mid-gestation. We identified thousands of enhancer contacts and found that most enhancer loci display tissue-specific 3D conformations. Moreover, developmental

enhancers display higher interaction frequencies with promoters and neighboring enhancers in tissues where they are active. We also show that invariant E—P interactions are rare and form independently of enhancer activity. More than 60% of developmental enhancers skip their immediate neighboring genes, which are often repressed, to instead contact a more distal gene suggesting a common mechanism for achieving E–P specificity. Our results provide a global view of tissue-specific enhancer 3D chromatin conformation and support the broad importance of E–P physical proximity for developmental gene activation.

Results

Enhancer interactome for 935 *in vivo* developmental enhancers across 10 mouse embryonic tissues

To create a map of *in vivo* enhancer-centric chromatin interactions in developing mouse embryos, we used the VISTA Enhancer Browser, a unique resource of human and mouse enhancers with *in vivo* activities experimentally validated in transgenic mice (Visel et al. 2006; Pennacchio et al. 2006). This resource verifies, and thus allows direct comparison of, tissue/cell types in which each tested enhancer is active or inactive. We created a sizable and robust core set of experimentally verified *in vivo* enhancers comprising 935 enhancers with highly reproducible activities in mouse embryonic tissues at mid-gestation (embryonic day 11.5). Tissues in which enhancers were active included the

forebrain, midbrain, hindbrain, neural tube, craniofacial structures, limb buds, heart and other tissues and cell types (see **Table S1** for details). To assess tissue-specific chromatin interactions centered on these enhancers, we collected 10 tissues from E11.5 mouse embryos (forebrain, midbrain, hindbrain, neural tube, face, forelimb, hindlimb, heart, tail and trunk) with two biological replicates per tissue, and performed the enhancer capture Hi-C assay (ecHi-C, **Fig. 1A** and **Methods**). This diverse tissue panel represents all major embryonic organs in which selected enhancers are active and for which extensive chromatin state maps (ATAC-seq, ChIP-seq for major histone modifications and DNA methylation) were created as part of the ENCODE project (Gorkin et al. 2020; ENCODE Project Consortium 2012). We designed RNA probes (Agilent SureSelect platform) targeting each of the 935 enhancers, as well as 176 promoters and 87 elements with no reproducible enhancer activity at E11.5 as negative controls (**Fig. 1A,** see **Methods** and **Table S1** for details).

After restriction fragment pooling and quality control we identified a total of 20,896 significant interactions across all tissues, ~80% of which were called within the same TAD (see **Fig. S1A-D**, **Table S2** and **Methods**). These interactions included E–P (2,818), enhancer–enhancer (E–E) (5,612), enhancer–CTCF (6,206) and other types of contacts (**Fig. S1D**). Most enhancers only interacted with one or two genes with a median distance between an enhancer and a target promoter of ~410 kb (**Fig. 1C** and **S1F**). For example, in the midbrain, the hs654 enhancer displayed the strongest significant interaction with

promoters of two adjacent genes, *Zic1 and Zic4,* located ~600 kb away. Reciprocally the viewpoint containing the *Zic1* and *Zic4* promoters (located ~3 kb from each other) also

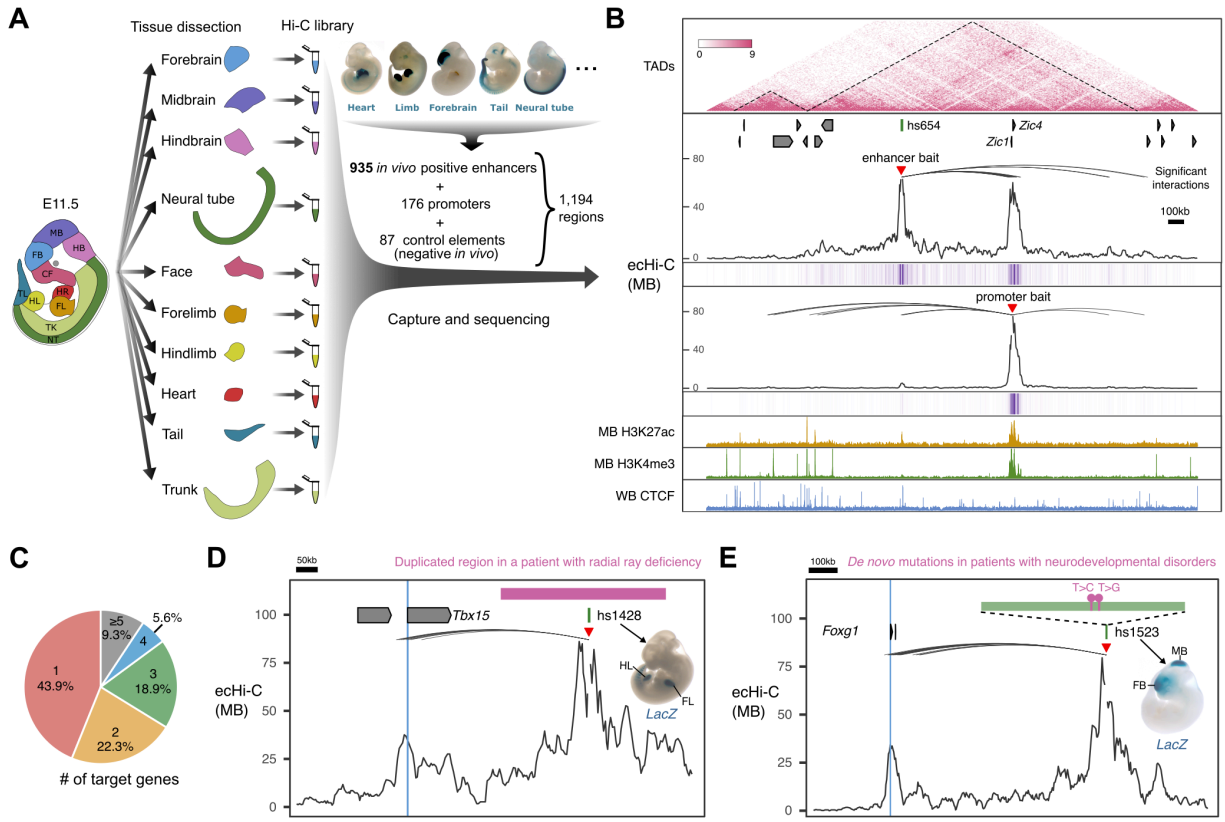

Figure 1: Identification of enhancer-centric chromatin interactions in 10 mouse embryonic tissues. (A) Experimental design. Tissue samples from E11.5 mouse embryos were used to prepare Hi-C libraries followed by oligonucleotide capture with probes targeting 1,224 baited regions, including 935 enhancers, 176 promoters and 87 control elements. **(B)** Enhancer capture Hi-C (ecHi-C) identifies chromatin interactions of enhancers. A 3 Mb region containing the hs654 midbrain enhancer (chr9:89500000-92500000; mm10) is shown with the following annotations from top to bottom: TADs (Jiang et al. 2017; Wang et al. 2018); Refseq genes; normalized hs654-centered (red arrowhead) chromatin interaction frequencies in midbrain (y-axis) shown as plot and purple heat map below; normalized *Zic1*/*Zic4*-promoter-centered (red arrowhead) chromatin interaction frequencies (y-axis); H3K27ac, H3K4me3 ChIP-seq, and DNAse-Seq profiles in midbrain (MB) at E11.5; CTCF ChIP-seq profile in whole brain (WB) at E12.5 (Gorkin et al. 2020; ENCODE Project Consortium 2012; Amândio et al. 2021). Curved lines indicate significant interactions. **(C)** Pie chart showing the percentage of enhancers interacting with different number of genes. **(D)** The hs1428 limb enhancer is in the non-coding region which is duplicated in patients with radial ray deficiency (pink box indicates homologous region in the mouse genome). Hs1428 forms significant chromatin interactions with the promoter of *Tbx15* located ~400 kb away (chr3:99,000,000-99,900,000; mm10). (**E**) Two *de novo* rare variants identified in patients with neurodevelopmental disorders are in the hs1523 forebrain/midbrain enhancer which forms strong significant interactions with the promoter of *Foxg1* located ~700 kb away (chr12:49,121,092-50,469,462; mm10).

showed significant interaction with the hs654 enhancer (**Fig. 1B**).

To provide orthogonal support for the functional relevance of identified chromatin interactions we compared them with ENCODE chromatin data that was generated for an overlapping set of tissues from E11.5 mouse embryos. We found that the 935 *in vivo* positive enhancers and 176 promoters contacted other elements annotated by ENCODE (promoters, enhancers, CTCF sites) significantly more often than the negative 87 control regions, thus supporting the enhancer interactions identified above (**Fig. S1E**).

We also identified significant tissue-specific chromatin interactions between enhancers containing mutations implicated in human congenital disorders and their known target genes in relevant tissues. These examples included non-coding regions involved in limb and craniofacial malformations, neurodevelopmental disorders and autism (**Figs. 1D, E** and **S2**, see **Table S3** for a full list of disease-associated chromatin interactions). For example, the hs1428 limb enhancer, located inside a region that is microduplicated in patients with radial ray deficiency, interacted with *Tbx15*, a key gene in limb development (**Fig. 1D**) (Flöttmann et al. 2018). The hs1877 enhancer, which is active in facial tissues and located in a region associated with cleft lip risk, interacted with *Myc* (**Fig. S2C**) (Uslu et al. 2014). We found that the hs737 enhancer, which contains several *de novo* variants linked to autism, interacted with *Ebf3* (**Fig. S2D**) (Padhi et al. 2021; Turner et al. 2017). EcHi-C also identified previously uncharacterized interacting genes for non-

coding regions implicated in congenital disorders (Short et al. 2018; Firth et al. 2009) (**Table S3**). One such region in humans contained two independent *de novo* variants (chr14:29390806T>C; chr14:29390876T>G; hg38) identified in patients with neurodevelopmental disorders. Both variants reside in the human hs1523 enhancer, but its regulatory target is unknown. Hs1523 is active in the telencephalon and midbrain (**Fig. 1E**) and is highly conserved across vertebrates (Visel et al. 2006). We found that Hs1523 formed strong brain-specific chromatin interactions with *Foxg1*, a gene implicated in Rett-like neurodevelopmental syndrome (Florian, Bahi-Buisson, and Bienvenu 2012; Ariani et al. 2008), thus establishing a likely mechanistic link between non-coding mutations from patients and a specific disease-causing gene. These results provide additional evidence for the specific regulatory connection between disease-associated enhancers and their *in vivo* target genes and further support E–P chromatin interactions identified by ecHi-C.

Long-range enhancer–promoter specificity is linked to repressed promoter state

Nearly 61% of enhancers in our study did not interact with the promoters of adjacent genes but instead contacted more distal genes (**Fig. 2A**). For example, the hs314 midbrain enhancer strongly interacts with the promoter of *Lhx2* located ~200 kb away but does not form any significant interactions with the more proximally located *Dennd1a* promoter (**Figs. 2B, C**). Similarly, a cluster of three forebrain enhancers, hs267, hs266 and hs853,

interacted with the *mir9-2* promoter located ~800 kb away, skipping over the more proximal *Tmem161b* promoter (**Fig. S6A**).

How is this E–P selectivity achieved in mammalian genomes? A recent study on a single mouse *Rex1/Fat1* locus suggests that promoter repression through DNA methylation may result in an intra-TAD E–P specificity (Ringel et al. 2022). To test if this mechanism is generally utilized at other developmental loci, we systematically assessed the chromatin state of skipped promoters. We focused on a subset of 556 enhancer-gene interactions identified by ecHi-C which bypass neighboring genes. Indeed, the expression of skipped genes was, on average, 56% lower than that of more distally located interacting genes (**Fig. 2D** and **S3A**). Skipped genes displayed substantially higher CpG methylation levels (**Fig. 2E** and **S3B**) and lower DNA accessibility (**Fig. 2F** and **S3C**) at their promoters than interacting genes. Interestingly, promoters of skipped genes did not display significantly

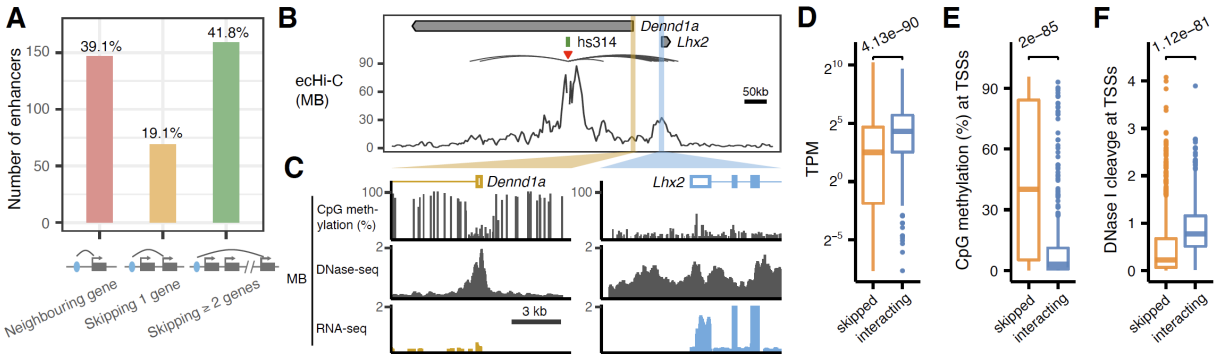

Figure 2: Properties of promoters that are skipped by remote enhancers. (**A**) Barplot showing E–P interactions grouped by genomic positions relative to the interacting genes. (**B**) The chromatin interaction profile of the hs314-enhancer (red arrowhead) is shown with significant interactions (black arches) in the midbrain at E11.5 (chr2:37,750,000-38,600,000; mm10). *Dennd1a* and *Lhx2* promoters are highlighted (brown and blue shading). (**C**) CpG methylation, DNase-seq and RNA-seq profiles at *Dennd1a* and *Lhx2* promoters in E11.5 midbrain (Gorkin et al. 2020; ENCODE Project Consortium 2012; Amândio et al. 2021; P. He et al. 2020). (**D-F**) The mRNA expression levels (D), CpG methylation (E) and DNase signal (F) of enhancer-interacting and skipped promoters in tissues where enhancers are active. MB, midbrain.

higher levels of trimethylation at histone H3 lysine 27 (H3K27me3) or lysine 9 (H3K9me3) (**Fig. S3D, E**), indicating that polycomb silencing and heterochromatin may not play a major role in regulating E–P selectivity. Taken together, our data indicate that promoters of skipped genes are often silenced.

5 **Enhancer knock-outs validate E–P chromatin interactions.**

While analysis of ecHi-C E–P chromatin interactions combined with *in vivo* reporter assays is strongly indicative of functional E-P gene interaction, they do not confirm that a given sequence is required for target gene expression. To assess the functionality of identified E–P chromatin interactions, we created enhancer knock-out mice for two
10 different genetic loci, *Zic1*/*Zic4* and *mir9-2* (**Fig. 3 and S4**). *Zic1* and *Zic4* are important for cerebellar development, and the loss of both genes causes the Dandy-Walker malformation (Grinberg et al. 2004; Ferraris et al. 2013; Blank et al. 2011). MiR-9 (together with miR-124) is the most abundant microRNA in mouse and human brains and is important for promoting neurogenesis (Coolen, Katz, and Bally-Cuif 2013; Yoo et al. 2011;
15 Shibata et al. 2011). We focused on the hs654 enhancer in the *Zic1*/*Zic4* locus and the hs267, hs266 and hs853 enhancer cluster in the *mir9-2* locus. All four enhancers are highly conserved in humans, and their human orthologs drive strong reproducible reporter gene expression in the developing mouse brain at E11.5 (**Fig. 4B**, **S4** and **S6A**). Furthermore,

all four enhancers form significant chromatin interactions with their putative target genes in the mouse embryonic brain at E11.5 (**Fig. 1B** and **S6A**).

We used CRISPR/Cas9 to create two mouse knock-out lines, one carrying a deletion of hs654 and the other carrying a deletion of the hs267/hs266/hs853 enhancers (**Fig. S4**). Mice homozygous for either deletion were born at normal Mendelian ratios, and no gross phenotypes or impairments were observed (**Fig. S4G**). To assess gene expression changes resulting from the loss of these enhancers, we sequenced polyadenylated RNA in the

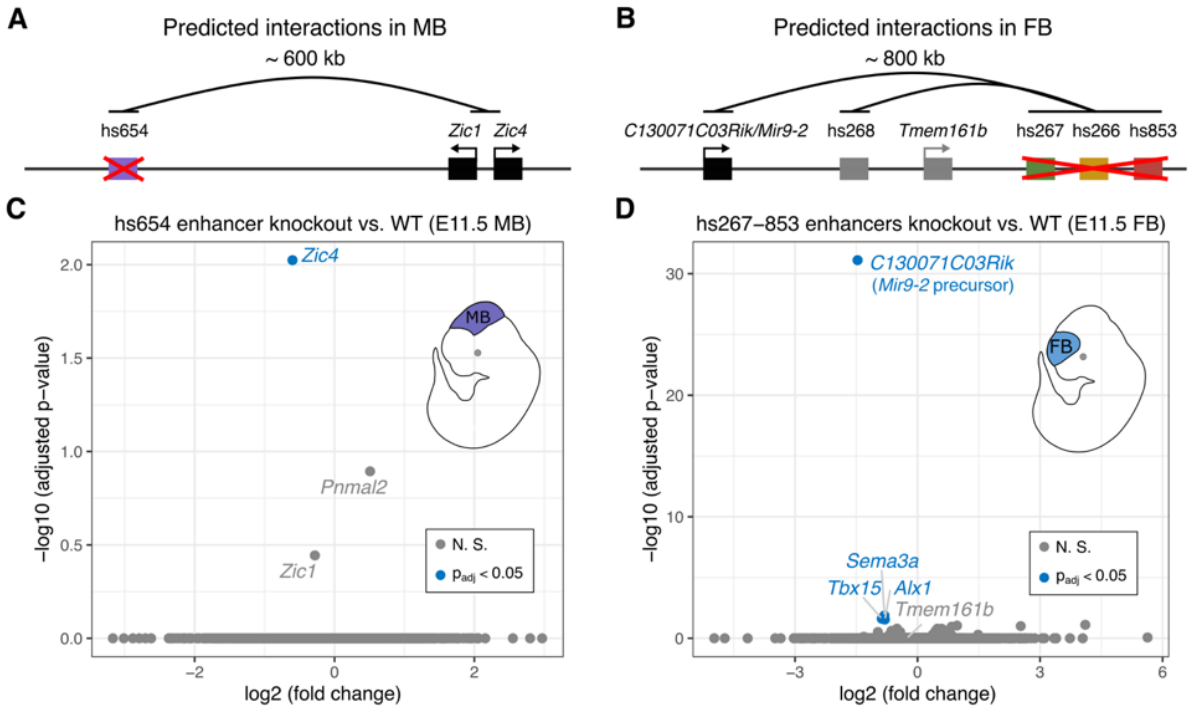

Fig. 3: Enhancers are required for the expression of interacting genes. Knock-out analysis of hs654 (A, C) and hs267/hs266/hs853 enhancers (B, D). (**A, B**) Predicted chromatin interactions are shown (black arches) to indicate enhancer target genes. Gene and enhancer models are not drawn to scale. (**C, D**) Transcriptome-wide mRNA expression changes in E11.5 whole midbrain of hs654 knock-out mice (C) and in E11.5 whole forebrain of hs267/hs266/hs853 knockout mice (D). Points indicate individual genes, with blue indicating statistically significant differences after adjustment for multiple comparisons (P_{adj} < 0.05, see the **Methods** for details).

midbrain (for *Δhs654* mice) and forebrain (for *Δhs267/hs266/hs853* mice) tissue from E11.5 mice from these enhancer deletion lines.

In mice homozygous null for hs654, *Zic4* RNA expression in the midbrain is reduced by ~34% compared with wild-type levels ($P_{adj} < 9.5 \times 10^{-3}$, **Fig. 3C**) supporting the functional relevance of the hs654-*Zic4* chromatin interaction in embryonic midbrain. This establishes *Zic4* as a direct regulatory target of hs654 and shows that the enhancer is required for normal expression of *Zic4* in the embryonic midbrain. *Zic1* expression was reduced by ~18%, albeit not statistically significant, and no other genes were significantly down- or upregulated in *Δhs654/Δhs654* mice (**Fig. 3C**).

Mice homozygous for the hs267/hs266/hs853 deletion show downregulation of *C130071C03Rik* (*mir9-2* precursor transcript) (Yang et al. 2017; Shibata et al. 2011; Tan et al. 2012; Zhao et al. 2009) by ~64% compared with the wild-type ($P_{adj} < 7.8 \times 10^{-32}$, **Fig. 3D**). Notably there was no significant change in *Tmem161b* expression or any other gene in *cis*, indicating that these three enhancers specifically control the expression of *mir9-2* as predicted by chromatin interactions between hs267/hs266/hs853 and the *mir9-2* promoter but not the *Tmem161b* promoter (**Fig. S6A**). Notably, neither enhancer deletion resulted in a complete loss of target gene expression, which is consistent with the presence of redundant enhancers at most developmental loci (**Fig. S6**) (Osterwalder et al. 2018; Kvon et al. 2021; Cannavò et al. 2016). Overall, the loss of enhancers results in a large decrease

in transcription of interacting target genes, which supports that E–P chromatin interactions identified by ecHi-C are functional.

Enhancer loops are stronger when enhancers are active

The general extent to which E–P interaction frequency correlates with *in vivo* enhancer activity at most developmental loci is unclear yet critical for understanding the spatio-temporal control of long-range gene regulation during development. To address this, we systematically compared tissue-specific enhancer activities with corresponding E–P interactions in different parts of the embryo. We selected 919 interacting E–P pairs identified by ecHi-C where gene expression matched enhancer activity in at least one tissue (see **Table S2** and **Methods**). We then systematically examined E–P chromatin interaction profiles in each of the ten tissues and compared them with the experimentally determined *in vivo* activities of corresponding enhancers in each of these tissues. Clustering of 919 E–P interactions across ten tissues revealed a strong correlation with *in vivo* enhancer activities (**Fig. 4A**). For example, enhancers active in the central nervous system displayed higher interaction frequencies in the forebrain, midbrain, hindbrain and neural tube but not in other tissues (**Fig. 4A**, cluster **a**). For instance, the hs654 enhancer that we showed directly regulates *Zic1*/*Zic4* genes (**Figs. 3A** and **4B**) drove reporter expression in the forebrain, midbrain, hindbrain and neural tube. Our ecHi-C experiments revealed that hs654 predominantly contacted *Zic1* and *Zic4* genes in the

brain, neural tube and tail, tissues where enhancer and gene were both active (**Fig. 4B**). Interaction between hs654 and *Zic1*/*Zic4* was largely absent in face, limbs and heart tissues where both hs654 and *Zic1*/*Zic4* are inactive (**Fig. 4B**) (Smith et al. 2014). Similarly, limb-specific enhancers displayed higher interaction frequencies in limb tissue (**Fig. 4A**, cluster **f**), heart-specific in the heart (**Fig. 4A**, cluster **d**), and face-specific in the face (**Fig. 4A**, cluster **e**). We observed this pattern – that enhancers form more frequent interactions with their respective target promoters when enhancers are active – for most enhancers in eight out of ten examined tissues (**Figs. 4C, D** and **S5A)**. There was no significant difference in interaction frequency for enhancers active in the tail and trunk, likely due to the low number of enhancers with characterized activity in these tissues (**Fig. S5A**). The enrichment of active interactions was stronger for active brain and neural tube enhancers that display stronger and more reproducible *in vivo* activity (**Fig. 4E** and **S5B** and **Methods**).

We observed a similar trend even within developmentally related tissues, such as different parts of the brain. Enhancers active only in specific areas of the developing brain, such as the forebrain or hindbrain, formed more frequent interactions with promoters in those tissues compared with parts of the brain where those enhancers were inactive (**Figs. S5D**, **E)**. Notably, a small fraction of enhancers that formed invariant interactions with promoters across all tissues displayed an increased frequency of these interactions in tissues where the enhancer was active *in vivo* (**Figs. S7A** and **B**). These results indicate

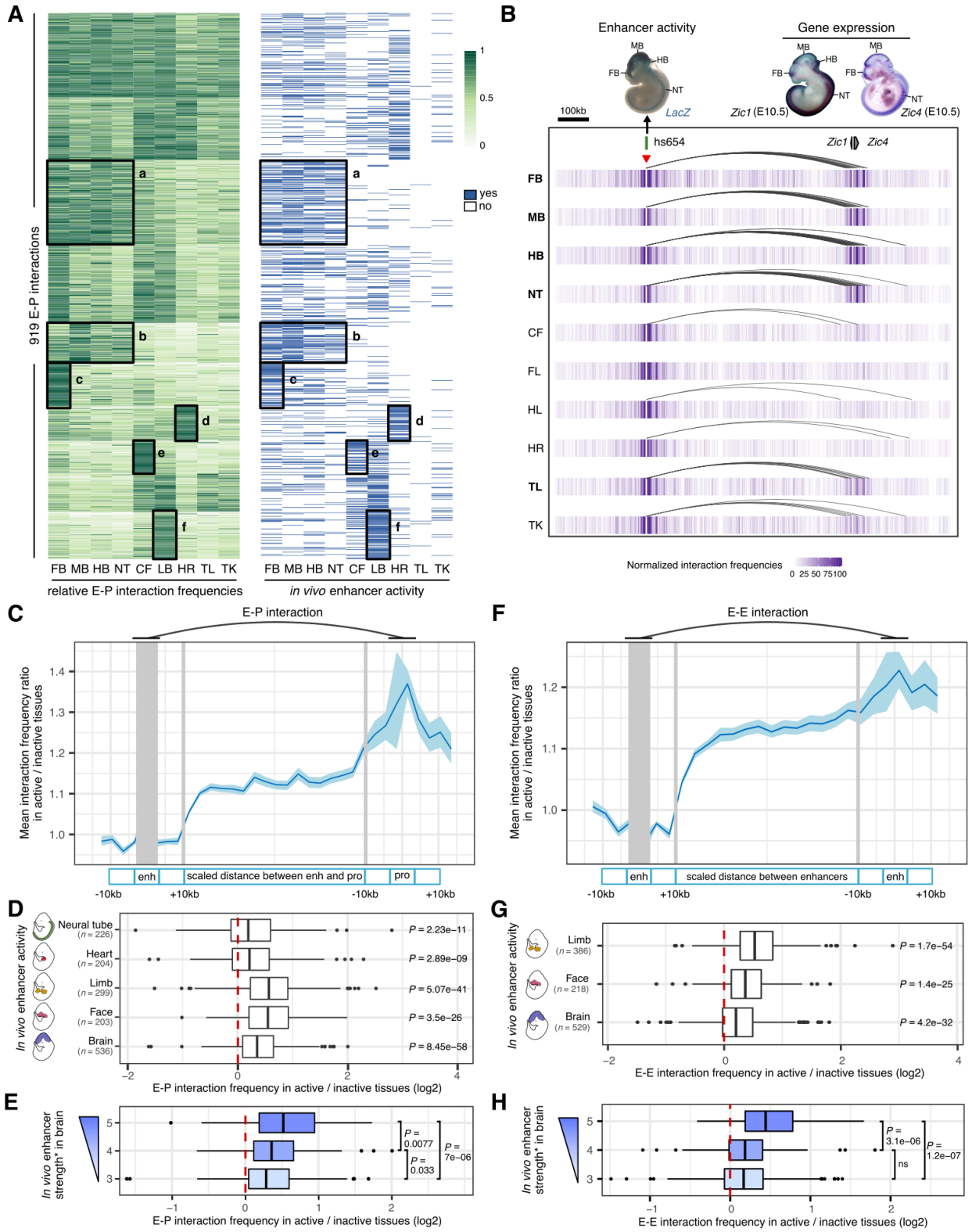
A
919 E-P interactions
a
b
c
d
e
f
FB MB HB NT CF LB HR TL TK
relative E-P interaction frequencies
in vivo enhancer activity
yes
no
B
Enhancer activity
Gene expression
MB
HB
FB
NT
LacZ
Zic1 (E10.5)
Zic4 (E10.5)
100kb
hs654
Zic1
Zic4
FB
MB
HB
NT
CF
FL
HL
HR
TL
TK
Normalized interaction frequencies
0 25 50 75100
C
E-P interaction
Mean interaction frequency ratio in active / inactive tissues
enh
scaled distance between enh and pro
pro
-10kb
+10kb
D
In vivo enhancer activity
Neural tube (n = 226)
Heart (n = 204)
Limb (n = 299)
Face (n = 203)
Brain (n = 536)
P = 2.23e−11
P = 2.89e−09
P = 5.07e−41
P = 3.5e−26
P = 8.45e−58
E-P interaction frequency in active / inactive tissues (log2)
E
In vivo enhancer strength* in brain
P = 0.0077
P = 0.033
P = 7e−06
E-P interaction frequency in active / inactive tissues (log2)
F
E-E interaction
Mean interaction frequency ratio in active / inactive tissues
enh
scaled distance between enhancers
enh
-10kb
+10kb
G
In vivo enhancer activity
Limb (n = 386)
Face (n = 218)
Brain (n = 529)
P = 1.7e−54
P = 1.4e−25
P = 4.2e−32
E-E interaction frequency in active / inactive tissues (log2)
H
In vivo enhancer strength* in brain
P = 3.1e−06
ns
P = 1.2e−07
E-E interaction frequency in active / inactive tissues (log2)

Figure 4: Tissue specificity of enhancer interactions in developing mouse embryo. (**A**) Heatmap showing relative E–P chromatin interaction frequencies (scaled to the max value among tissues in each interaction, green) and the *in vivo* enhancer activities (blue) of 919 E–P chromatin interactions. *k*-means clustering (k = 10) was performed on interaction frequencies. The six highlighted tissue-specific interaction clusters match *in vivo* enhancer activities. (**B**) Interaction profiles across 10 tissues centered on the hs654 enhancer (red arrowhead). The top left shows hs654 enhancer activity in a transgenic mid-gestation (E11.5) mouse embryo (chr9:90,390,345-91,695,319). Top right image shows *Zic1* and *Zic4* mRNA whole-mount *in situ* hybridization (WISH) at E10.5 (Images have been reproduced with permission from Gene Expression Database (GXD; *Zic4*) (Smith et al. 2014) and Embrys database (http://embrys.jp; *Zic1*). Heatmaps with normalized interaction frequencies in each of the 10 tissues are shown below. Curved lines indicate significant interactions. (**C**) Average ratio of E–P interaction frequency between active and inactive tissues based on the analysis of 896 E–P chromatin interactions is shown (see **Methods** for details of normalization procedure). To construct a metaplot profile, interaction frequencies were scaled as follows: (1) the 5′ end (10 kb around the midpoint of baited enhancer) and the 3′ end (10 kb around the midpoint of interacting promoters) were unscaled; (2) the regions between them have been scaled to 100 kb. Light blue shading indicates 95% confidence intervals estimated by non-parametric bootstrapping. (**D**) Average ratio of enhancer-promoter interaction frequency between active and inactive tissues for enhancers active in different tissues (see **Fig. S5A** for all ten tissues). (**E**) Average ratio of enhancer-promoter interaction frequency between active and inactive tissues for brain enhancers with different strength (see **Fig. S5B** for other tissues). (**F**) Average ratio of enhancer–enhancer interaction frequency between active and inactive tissues based on the analysis of 934 E–E chromatin interactions is shown (see **Methods** for details). Light blue shading indicates 95% confidence intervals estimated by non-parametric bootstrapping. (**G**) Average ratio of E–E interaction frequency between active and inactive tissues for enhancers active in neural tube, heart, limb, face and brain (see **Fig. S8B** for other tissues). (**H**) Average ratio of E–E interaction frequency between active and inactive tissues for brain enhancers of different strength (see **Fig. S8C** for other tissues). *P* values were calculated by paired-sample two-sided Wilcox test and adjusted for multiple testing for interaction frequencies comparison between active and inactive tissues, unpaired-sample two-sided Wilcox test was performed on comparison among different enhancer strength. FB, forebrain. MB, midbrain. HB, hindbrain. CF, craniofacial mesenchyme. HR, heart. FL, forelimb. HL, hindlimb. TK, trunk. TL, tail. NT, neural tube.

that increasing the interaction frequency with the target gene is needed for the enhancer to activate transcription even though a pre-formed topology exists (Williamson et al. 2016).

We next examined *in vivo* chromatin interactions between enhancers (E—E contacts), including enhancers predicted based on chromatin features such as H3K27ac. Previous studies suggest a model in which enhancers regulating the same gene in the same cell form multi-enhancer hubs to activate gene expression (Kvon et al. 2021; Tsai, Alves, and

Crocker 2019; Hnisz et al. 2017; Madsen et al. 2020). However, the extent to which these interactions occur *in vivo* between developmental enhancers in mammals remains unknown. We observed that E—E contacts formed between enhancers with overlapping activities are likely to regulate the same gene (**Fig. S6**). For example, the hs268, hs267, hs266 and hs853 enhancers, which are located in the same TAD, formed extensive significant interactions with the promoter of the *mir9-2* gene (**Fig. S6A**). All four enhancers were active in the dorsal telencephalon, and their activity patterns were strikingly similar to the expression of the *mir9-2* precursor (**Figs. S6A, C**). All four enhancers also formed extensive interactions with each other in the forebrain (**Fig. S6A**), but these E–E interactions were virtually absent in developing limb buds where *mir9-2* is not expressed, suggesting that these four enhancers form a multi-enhancer hub (**Fig. S6B**). We observed similar tissue-specific E–E interactions at other loci and tissues e.g., enhancers active in the developing face at the *Msx1* locus and enhancers active in the neural tube at the *Tfap2a* locus (**Figs. S6D, E**). Generally, enhancers formed stronger interactions with other enhancers when they were active in the brain, face or limb (**Figs. 4F, G** and **S8B**). These results are consistent with a model in which increased physical proximity among multiple enhancers during mammalian development and a given promoter accompanies transcriptional activation.

Invariant E–P interactions are rare, linked to CTCF binding, and likely form independently of enhancer activity

Widespread stable mammalian E–P loops have been reported for enhancers, predicted from chromatin features in mouse embryonic limb and brain (Andrey et al. 2017), mouse embryonic stem cells (Kubo et al. 2021; Rao et al. 2014), and human keratinocytes (Rubin et al. 2017). However, how common is stable E–P looping at most developmental loci is unknown. Our analysis of E–P chromatin interactions for *bona fide* developmental enhancers found that only a small fraction (13.6%) formed tissue-invariant loops across all ten examined embryonic tissues (**Figs. 5A-D**). Stable E–P chromatin interactions are typically associated with neighboring CTCF binding (Andrey et al. 2017; Rao et al. 2014), especially for long-range E–P contacts such as ZRS-*Shh* (Kubo et al. 2021; Paliou et al. 2019). Indeed, we observed that tissue-invariant interactions are also associated with proximal CTCF binding, with more than 85% of all invariant interactions having proximal (< 5 kb) CTCF binding at either end, including the ZRS-*Shh* locus (**Fig. 5C** and **E**).

Interestingly, these invariant E–P chromatin interactions did not correlate with enhancer activity, as the vast majority of enhancers that formed these interactions were active only in a small subset of tissues, with the number of tissues they are active in similar to

enhancers that form tissue-specific contacts (**Fig. S7C**), suggesting that invariant interactions might form independently of enhancer activity.

To test if tissue-invariant interactions form independently of enhancer activity, we experimentally assessed how these E–P chromatin contacts are affected by targeted deletion of the enhancer. We chose the *Shh* locus where a limb-specific ZRS enhancer forms chromatin interactions with the *Shh* promoter located ~850 kb away in all ten examined tissues (**Fig. 5C**). We generated a knock-in mouse line in which the entire ZRS enhancer was replaced with a piece of non-mouse DNA lacking any regulatory activity to simultaneously get rid of the enhancer and enable allele-specific detection of chromatin interactions in the ecHi-C experiments. For that purpose, we used part of the bacterial *lacZ* gene sequence. Mice homozygous for the ZRS^{lacZ} allele showed no detectable *Shh* expression in the limb buds and displayed reduced limb buds at E11.5 and truncated zeugopods and autopods at E18.5, which is consistent with complete loss of Shh function in the limb (**Figs. 5F** and **S9**) (Sagai et al. 2005; Kvon et al. 2016). To determine whether ZRS enhancer activity contributes to its higher-order chromatin interactions with the *Shh* promoter we performed capture Hi-C experiments in limb buds of E11.5 mice heterozygous for the ZRS^{lacZ} allele. An advantage of using heterozygous mice is that limbs are formed normally (Sagai et al. 2005) and chromatin interactions are assessed in fully developed limb bud tissue. We used probes targeting both the wild-type ZRS and LacZ sequence, which allowed us to directly compare the chromatin interactions of the *Shh*

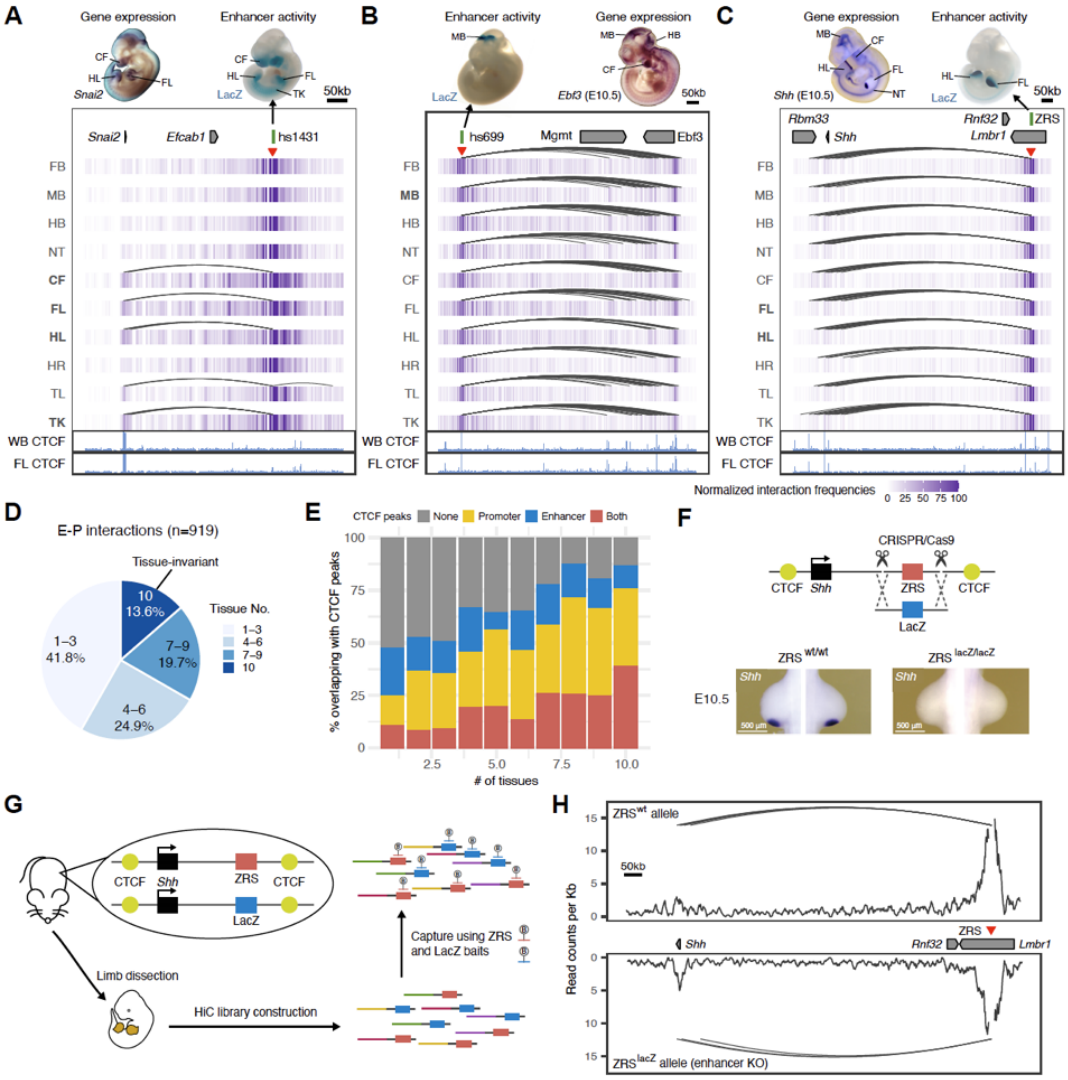

Figure 5: Properties of tissue-invariant enhancer–promoter chromatin interactions. (**A-C**) Chromatin interaction profiles across 10 tissues centered on the hs1431 enhancer in the *Snai2* locus (chr16:14,610,000-15,220,000; mm10) (A), the hs699 enhancer in the *Dlx5/6* locus (chr7: 136,400,000-137,400,000; mm10) (B) and the ZRS enhancer in the *Shh* locus (chr5:28,320,000-29,400,000; mm10) (C). Shown above are corresponding enhancer activities in transgenic E11.5 mouse embryos and corresponding interacting gene mRNA WISH in E11.5 or E10.5 embryos. Heatmaps with normalized interaction frequencies in each of the 10 tissues are shown below. CTCF ChIP-seq profiles (blue) in the whole brain (WB) and forelimb (FL) at E12.5 are shown at the bottom. Arches indicate significant interactions. Red arrowheads depict ecHi-C viewpoints. (**D**) Pie chart showing the fraction of E–P interactions present in different numbers of tissues. (**E**) Fraction of E–P interactions that overlap with CTCF peaks grouped by number of tissues in which interaction was detected. (**F**) Cas9-mediated replacement of the mouse ZRS sequence with a fragment of bacterial LacZ gene. *Shh* mRNA WISH analysis in wild type and $ZRS^{LacZ/LacZ}$ E10.5 mouse forelimb buds. See **Fig. S9** for details**.** (**G**) Schematic overview of the capture Hi-C approach to detect chromatin interactions in the presence and absence of the ZRS in limbs of the same mouse using RNA probes targeting ZRS and LacZ. (**H**) Allele-specific ZRS-region-centric chromatin interactions in limb buds of E11.5 $ZRS^{+/LacZ}$ mice. WISH images in A and B have been reproduced with permission from Gene Expression Database (GXD, *Ebf3*) (Smith et al. 2014) and Embrys database (http://embrys.jp; *Snai2*)

promoter with both alleles in the same mouse (**Fig. 5G**). We found that both the wild-type ZRS allele and enhancerless lacZ allele formed significant interactions with the *Shh* promoter (**Fig. 5H**). These results demonstrate that the higher-order chromatin interaction between ZRS and *Shh* can form independently of ZRS enhancer activity.

Conclusions

In this study, we comprehensively determined the tissue-resolved *in vivo* interaction landscapes for 935 *bona fide* enhancers, thus revealing thousands of tissue-specific interactions. Enhancer 3D chromatin conformations are highly dynamic across tissues, which mirrors the highly tissue-specific activity patterns that have been observed for these enhancers for a long time. We find that the strongest E–P and E–E interactions are formed where enhancers are functionally active. Widespread developmental E–E contacts are consistent with the observation that most developmental genes are controlled by multiple enhancers with overlapping activities (Osterwalder et al. 2018; Montavon et al. 2011; Perry et al. 2010; Frankel et al. 2010; Wunderlich et al. 2016; Kvon et al. 2021; Dickel et al. 2018) and the concept of multi-enhancer 'hubs' (Madsen et al. 2020; Tsai, Alves, and Crocker 2019; Hnisz et al. 2017). Together, our chromatin interaction data for 935 enhancers suggest that E–P physical proximity is a general and important feature of developmental gene activation in mammals. These results contrast with other developmental systems such as early *Drosophila* embryo development (Ghavi-

Helm et al. 2014; Espinola et al. 2021; Simmons et al. 2021) or stimulus-induced gene activation where E–P loops appear to be stable and likely to ensure robust and rapid gene activation (Platt et al. 2016; Rodríguez-Carballo et al. 2020). The average observed increase in E–P contact frequency between active and inactive tissues appears to be less than 1.5-fold (**Fig. 4C**), even though average changes in associated tissue-specific gene expression are ~11-fold (**Fig. S5C**). The lack of cellular resolution in detecting specific chromatin interactions in our study could explain the relatively subtle differences in observed contact frequencies. Indeed, stronger active enhancers display larger differences in contact frequencies. However, even for the strongest active enhancers, the average difference in contact frequency compared to inactive tissues is less than twofold (**Fig. 4C** and **S5A**). These results are consistent with studies in fly embryo single cells that showed a 1-2.5-fold increase in contact frequency between enhancers and promoters after disruption of TAD borders results in more than 10-fold transcriptional change (Xiao, Hafner, and Boettiger 2021), suggesting that transcription is hypersensitive to changes in contact frequency across species. Several models have been proposed to explain this nonlinear relationship between E–P contact probability and transcription, including bistability, hysteresis, and transient two-state E–P interactions (Zuin et al. 2022; Xiao, Hafner, and Boettiger 2021). Our data support subtle but consistent changes in E–P contact frequency upon enhancer activation, highlighting the general significance of E–P physical proximity for developmental gene regulation in mammals.

Notably, we also detected E–P chromatin interactions that are tissue-invariant and are associated with proximal CTCF binding. Similar stable loops have been reported for other mammalian loci (Andrey et al. 2017; Rubin et al. 2017; Jin et al. 2013; Paliou et al. 2019) where it likely provides an additional level of robustness to maintain stable levels of gene expression during development (Paliou et al. 2019; Williamson et al. 2016). Our data on *bona fide* enhancers suggests that these interactions only form next to a minority of developmental enhancers and likely form independently of enhancer activity (**Fig. 5D-H**). Since both tissue-invariant CTCF/cohesin-bound loops formed by loop extrusion and enhancer loops are widespread in the genome (Lieberman-Aiden et al. 2009; Hsieh et al. 2021), it is plausible that many of them overlap. Indeed, we did not observe differences in tissue specificity, evolutionary DNA conservation, or classes of target genes between enhancers that form tissue-invariant chromatin contacts and enhancers that form tissue-specific chromatin interactions with their promoters (**Fig. S7C-E**). Despite this, invariant E–P interactions displayed higher interaction frequency in tissues where enhancers were active (**Fig. S7A, B**). Super-resolution imaging of the invariant E–P loop at the *Shh* locus (Williamson et al. 2016) suggests that the ZRS enhancer colocalizes with its target gene only in cells where the gene is active, further supporting that higher resolution C-methods and imaging techniques (Hua et al. 2021; Mateo et al. 2019) will be needed to untangle complex relationships between active enhancer and adjacent CTCF-mediated

looping. Overall, E–P physical proximity appears to be a general feature of mammalian developmental gene activation.

More than half of developmental enhancers in our study appear to skip neighboring genes to regulate a more distal one. Such interactions have also been reported in mice (Smemo et al. 2014; Fulco et al. 2019; Birnbaum et al. 2012), human (Lettice et al. 2003; Mifsud et al. 2015; Li et al. 2012; Gröschel et al. 2014; Visser, Kayser, and Palstra 2012), and to a lesser degree in Drosophila (Kvon et al. 2014; Calhoun, Stathopoulos, and Levine 2002). This raises the question: How is this E–P selectivity achieved? In *Drosophila* E–P specificity is regulated through compatibility between enhancers and different types of core promoters (Juven-Gershon and Kadonaga 2010; Zabidi et al. 2014; van Arensbergen, van Steensel, and Bussemaker 2014; Serebreni and Stark 2021; Galouzis and Furlong 2022). However, intrinsic E–P compatibility appears to play a lesser role in mammals where most enhancers activate all promoters by similar amounts (Bergman et al. 2022; Martinez-Ara et al. 2022; Zabidi et al. 2014). Another potential mechanism for achieving divergent gene expression patterns within the same TAD could be promoter repression via CpG methylation, as was recently shown in the mouse *Rex1*/*Fat1* locus (Ringel et al. 2022). Our analysis of remote E–P interactions shows that promoters of skipped genes are often inactive, methylated, and inaccessible (**Fig. 2D-F** and **S3**), suggesting that promoter repression could indeed be a widespread mechanism by which such enhancer–gene specificity is achieved in mammals. An additional mechanism may be tethering elements

(Calhoun, Stathopoulos, and Levine 2002; Batut et al. 2022; Pachano et al. 2021) which can facilitate formation and stabilization of specific E–P interactions. The general mechanism that determines E–P specificity in mammalian genomes is still poorly understood (van Arensbergen, van Steensel, and Bussemaker 2014; Galouzis and Furlong 2022), and further studies are needed to dissect how divergent expression is achieved within the same TAD.

Beyond insights into enhancer chromatin interactions, our study independently confirmed and identified novel putative *in vivo* target genes for enhancers that have been implicated in craniofacial and limb malformations, neurodevelopmental disorders, autism, and other disorders (**Figs. 1D, E** and **S2**, **Table S3**), demonstrating the utility of this resource to understand human congenital disorders and laying the groundwork for future in-depth studies of associated misregulated molecular pathways. It is important to note that the current study surveyed a relatively small fraction of *bona fide* developmental enhancers in a limited number of mouse embryonic tissues and timepoints. In future studies, functional characterization of a greater number of developmental enhancers and their chromatin interactions *in vivo* in various tissue and cell contexts will greatly aid functional interpretation of germline variants associated with human congenital disorders. Nonetheless, the current study provides a broad snapshot of the general 3D chromatin organization and properties of enhancers at typical developmental loci.

References

Alexander, Jeffrey M., Juan Guan, Bingkun Li, Lenka Maliskova, Michael Song, Yin Shen, Bo Huang, Stavros Lomvardas, and Orion D. Weiner. 2019. "Live-Cell Imaging Reveals Enhancer-Dependent Sox2 Transcription in the Absence of Enhancer Proximity." *ELife* 8 (May): e41769.

Amândio, Ana Rita, Leonardo Beccari, Lucille Lopez-Delisle, Bénédicte Mascrez, Jozsef Zakany, Sandra Gitto, and Denis Duboule. 2021. "Sequential in Cis Mutagenesis in Vivo Reveals Various Functions for CTCF Sites at the Mouse HoxD Cluster." *Genes & Development* 35 (21–22): 1490–1509.

Andrey, Guillaume, Thomas Montavon, Bénédicte Mascrez, Federico Gonzalez, Daan Noordermeer, Marion Leleu, Didier Trono, François Spitz, and Denis Duboule. 2013. "A Switch between Topological Domains Underlies HoxD Genes Collinearity in Mouse Limbs." *Science* 340 (6137): 1234167.

Andrey, Guillaume, Robert Schöpflin, Ivana Jerković, Verena Heinrich, Daniel M. Ibrahim, Christina Paliou, Myriam Hochradel, et al. 2017. "Characterization of Hundreds of Regulatory Landscapes in Developing Limbs Reveals Two Regimes of Chromatin Folding." *Genome Research* 27 (2): 223–33.

Arensbergen, Joris van, Bas van Steensel, and Harmen J. Bussemaker. 2014. "In Search of the Determinants of Enhancer–Promoter Interaction Specificity." *Trends in Cell Biology* 24 (11): 695–702.

Ariani, Francesca, Giuseppe Hayek, Dalila Rondinella, Rosangela Artuso, Maria Antonietta Mencarelli, Ariele Spanhol-Rosseto, Marzia Pollazzon, et al. 2008. "FOXG1 Is Responsible for the Congenital Variant of Rett Syndrome." *American Journal of Human Genetics* 83 (1): 89–93.

Attanasio, Catia, Alex S. Nord, Yiwen Zhu, Matthew J. Blow, Zirong Li, Denise K. Liberton, Harris Morrison, et al. 2013. "Fine Tuning of Craniofacial Morphology by Distant-Acting Enhancers." *Science* 342 (6157): 1241006.

Batut, Philippe J., Xin Yang Bing, Zachary Sisco, João Raimundo, Michal Levo, and Michael S. Levine. 2022. "Genome Organization Controls Transcriptional Dynamics during Development." *Science* 375 (6580): 566–70.

Benabdallah, Nezha S., Iain Williamson, Robert S. Illingworth, Lauren Kane, Shelagh Boyle, Dipta Sengupta, Graeme R. Grimes, Pierre Therizols, and Wendy A. Bickmore. 2019. "Decreased Enhancer-Promoter Proximity Accompanying Enhancer Activation." *Molecular Cell* 76 (3): 473-484.e7.

Bergman, Drew T., Thouis R. Jones, Vincent Liu, Judhajeet Ray, Evelyn Jagoda, Layla Siraj, Helen Y. Kang, et al. 2022. "Compatibility Rules of Human Enhancer and Promoter Sequences." *Nature* 607 (7917): 176–84.

Bhatia, Shipra, Hemant Bengani, Margaret Fish, Alison Brown, Maria Teresa Divizia, Riccardo de Marco, Guiseppe Damante, Robert Grainger, Veronica van Heyningen, and Dirk A. Kleinjan. 2013. "Disruption of Autoregulatory Feedback by a Mutation in a Remote, Ultraconserved PAX6 Enhancer Causes Aniridia." *American Journal of Human Genetics* 93 (6): 1126–34.

Birnbaum, Ramon Y., David B. Everman, Karl K. Murphy, Fiorella Gurrieri, Charles E. Schwartz, and Nadav Ahituv. 2012. "Functional Characterization of Tissue-Specific Enhancers in the DLX5/6 Locus." *Human Molecular Genetics* 21 (22): 4930–38.

Blank, Marissa C., Inessa Grinberg, Emmanuel Aryee, Christine Laliberte, Victor V. Chizhikov, R. Mark Henkelman, and Kathleen J. Millen. 2011. "Multiple Developmental Programs Are Altered by Loss of Zic1 and Zic4 to Cause Dandy-Walker Malformation Cerebellar Pathogenesis." *Development* 138 (6): 1207–16.

Bulger, M., and M. Groudine. 1999. "Looping versus Linking: Toward a Model for Long-Distance Gene Activation." *Genes & Development* 13 (19): 2465–77.

Cairns, Jonathan, Paula Freire-Pritchett, Steven W. Wingett, Csilla Várnai, Andrew Dimond, Vincent Plagnol, Daniel Zerbino, et al. 2016. "CHiCAGO: Robust Detection of DNA Looping Interactions in Capture Hi-C Data." *Genome Biology* 17 (1): 127.

Cairns, Jonathan, William R. Orchard, Valeriya Malysheva, and Mikhail Spivakov. 2019. "Chicdiff: A Computational Pipeline for Detecting Differential Chromosomal Interactions in Capture Hi-C Data." *Bioinformatics* 35 (22): 4764–66.

Calhoun, Vincent C., Angelike Stathopoulos, and Michael Levine. 2002. "Promoter-Proximal Tethering Elements Regulate Enhancer-Promoter Specificity in the Drosophila Antennapedia Complex." *Proceedings of the National Academy of Sciences of the United States of America* 99 (14): 9243–47.

Cannavò, Enrico, Pierre Khoueiry, David A. Garfield, Paul Geeleher, Thomas Zichner, E. Hilary Gustafson, Lucia Ciglar, Jan O. Korbel, and Eileen E. M. Furlong. 2016. "Shadow Enhancers Are Pervasive Features of Developmental Regulatory Networks." *Current Biology: CB* 26 (1): 38–51.

Coolen, Marion, Shauna Katz, and Laure Bally-Cuif. 2013. "MiR-9: A Versatile Regulator of Neurogenesis." *Frontiers in Cellular Neuroscience* 7 (November): 220.

Deng, Wulan, Jongjoo Lee, Hongxin Wang, Jeff Miller, Andreas Reik, Philip D. Gregory, Ann Dean, and Gerd A. Blobel. 2012. "Controlling Long-Range Genomic Interactions at a Native Locus by Targeted Tethering of a Looping Factor." *Cell* 149 (6): 1233–44.

Deng, Wulan, Jeremy W. Rupon, Ivan Krivega, Laura Breda, Irene Motta, Kristen S. Jahn, Andreas Reik, et al. 2014. "Reactivation of Developmentally Silenced Globin Genes by Forced Chromatin Looping." *Cell* 158 (4): 849–60.

Dickel, Diane E., Iros Barozzi, Yiwen Zhu, Yoko Fukuda-Yuzawa, Marco Osterwalder, Brandon J. Mannion, Dalit May, et al. 2016. "Genome-Wide Compendium and Functional Assessment of in Vivo Heart Enhancers." *Nature Communications* 7 (October): 12923.

Dickel, Diane E., Athena R. Ypsilanti, Ramón Pla, Yiwen Zhu, Iros Barozzi, Brandon J. Mannion, Yupar S. Khin, et al. 2018. "Ultraconserved Enhancers Are Required for Normal Development." *Cell* 172 (3): 491-499.e15.

Dixon, Jesse R., Siddarth Selvaraj, Feng Yue, Audrey Kim, Yan Li, Yin Shen, Ming Hu, Jun S. Liu, and Bing Ren. 2012. "Topological Domains in Mammalian Genomes Identified by Analysis of Chromatin Interactions." *Nature* 485 (7398): 376–80.

Dobin, Alexander, Carrie A. Davis, Felix Schlesinger, Jorg Drenkow, Chris Zaleski, Sonali Jha, Philippe Batut, Mark Chaisson, and Thomas R. Gingeras. 2013. "STAR: Ultrafast Universal RNA-Seq Aligner." *Bioinformatics* 29 (1): 15–21.

Dryden, Nicola H., Laura R. Broome, Frank Dudbridge, Nichola Johnson, Nick Orr, Stefan Schoenfelder, Takashi Nagano, et al. 2014. "Unbiased Analysis of Potential Targets of Breast Cancer Susceptibility Loci by Capture Hi-C." *Genome Research* 24 (11): 1854–68.

ENCODE Project Consortium. 2012. "An Integrated Encyclopedia of DNA Elements in the Human Genome." *Nature* 489 (7414): 57–74.

ENCODE Project Consortium, Jill E. Moore, Michael J. Purcaro, Henry E. Pratt, Charles B. Epstein, Noam Shoresh, Jessika Adrian, et al. 2020. "Expanded Encyclopaedias of DNA Elements in the Human and Mouse Genomes." *Nature* 583 (7818): 699–710.

Espinola, Sergio Martin, Markus Götz, Maelle Bellec, Olivier Messina, Jean-Bernard Fiche, Christophe Houbron, Matthieu Dejean, et al. 2021. "Cis-Regulatory Chromatin Loops Arise before TADs and Gene Activation, and Are Independent of Cell Fate during Early Drosophila Development." *Nature Genetics* 53 (4): 477–86.

Fakhouri, Walid D., Fedik Rahimov, Catia Attanasio, Evelyn N. Kouwenhoven, Renata L. Ferreira De Lima, Temis Maria Felix, Larissa Nitschke, et al. 2014. "An Etiologic Regulatory Mutation in IRF6 with Loss- and Gain-of-Function Effects." *Human Molecular Genetics* 23 (10): 2711–20.

Ferraris, Alessandro, Laura Bernardini, Vesna Sabolic Avramovska, Ginevra Zanni, Sara Loddo, Elena Sukarova-Angelovska, Valentina Parisi, et al. 2013. "Dandy-Walker Malformation and Wisconsin Syndrome: Novel Cases Add Further Insight into the Genotype-Phenotype Correlations of 3q23q25 Deletions." *Orphanet Journal of Rare Diseases* 8 (May): 75.

Firth, Helen V., Shola M. Richards, A. Paul Bevan, Stephen Clayton, Manuel Corpas, Diana Rajan, Steven Van Vooren, Yves Moreau, Roger M. Pettett, and Nigel P. Carter. 2009. "DECIPHER: Database of Chromosomal Imbalance and Phenotype in Humans Using Ensembl Resources." *American Journal of Human Genetics* 84 (4): 524–33.

Florian, C., N. Bahi-Buisson, and T. Bienvenu. 2012. "FOXG1-Related Disorders: From Clinical Description to Molecular Genetics." *Molecular Syndromology* 2 (3–5): 153–63.

Flöttmann, Ricarda, Bjørt K. Kragesteen, Sinje Geuer, Magdalena Socha, Lila Allou, Anna Sowińska-Seidler, Laure Bosquillon de Jarcy, et al. 2018. "Noncoding Copy-Number Variations Are Associated with Congenital Limb Malformation." *Genetics in Medicine: Official Journal of the American College of Medical Genetics* 20 (6): 599–607.

Franke, Martin, Daniel M. Ibrahim, Guillaume Andrey, Wibke Schwarzer, Verena Heinrich, Robert Schöpflin, Katerina Kraft, et al. 2016. "Formation of New Chromatin Domains Determines Pathogenicity of Genomic Duplications." *Nature* 538 (7624): 265–69.

Frankel, Nicolás, Gregory K. Davis, Diego Vargas, Shu Wang, François Payre, and David L. Stern. 2010. "Phenotypic Robustness Conferred by Apparently Redundant Transcriptional Enhancers." *Nature* 466 (7305): 490–93.

Freire-Pritchett, Paula, Helen Ray-Jones, Monica Della Rosa, Chris Q. Eijsbouts, William R. Orchard, Steven W. Wingett, Chris Wallace, Jonathan Cairns, Mikhail Spivakov, and Valeriya Malysheva. 2021. "Detecting Chromosomal Interactions in Capture Hi-C Data with CHiCAGO and Companion Tools." *Nature Protocols*, August, 1–39.

Freire-Pritchett, Paula, Stefan Schoenfelder, Csilla Várnai, Steven W. Wingett, Jonathan Cairns, Amanda J. Collier, Raquel García-Vílchez, et al. 2017. "Global Reorganisation of Cis-Regulatory Units upon Lineage Commitment of Human Embryonic Stem Cells." *ELife* 6 (March). https://doi.org/10.7554/eLife.21926.

Fulco, Charles P., Joseph Nasser, Thouis R. Jones, Glen Munson, Drew T. Bergman, Vidya Subramanian, Sharon R. Grossman, et al. 2019. "Activity-by-Contact Model of Enhancer–Promoter Regulation from Thousands of CRISPR Perturbations." *Nature Genetics* 51 (12): 1664–69.

Furlong, Eileen E. M., and Michael Levine. 2018. "Developmental Enhancers and Chromosome Topology." *Science* 361 (6409): 1341–45.

Galouzis, Charalampos Chrysovalantis, and Eileen E. M. Furlong. 2022. "Regulating Specificity in Enhancer–Promoter Communication." *Current Opinion in Cell Biology* 75 (April): 102065.

Ghavi-Helm, Yad, Felix A. Klein, Tibor Pakozdi, Lucia Ciglar, Daan Noordermeer, Wolfgang Huber, and Eileen E. M. Furlong. 2014. "Enhancer Loops Appear Stable during Development and Are Associated with Paused Polymerase." *Nature* 512 (7512): 96–100.

Gorkin, David U., Iros Barozzi, Yuan Zhao, Yanxiao Zhang, Hui Huang, Ah Young Lee, Bin Li, et al. 2020. "An Atlas of Dynamic Chromatin Landscapes in Mouse Fetal Development." *Nature* 583 (7818): 744–51.

Grinberg, Inessa, Hope Northrup, Holly Ardinger, Chitra Prasad, William B. Dobyns, and Kathleen J. Millen. 2004. "Heterozygous Deletion of the Linked Genes ZIC1 and ZIC4 Is Involved in Dandy-Walker Malformation." *Nature Genetics* 36 (10): 1053–55.

Gröschel, Stefan, Mathijs A. Sanders, Remco Hoogenboezem, Elzo de Wit, Britta A. M. Bouwman, Claudia Erpelinck, Vincent H. J. van der Velden, et al. 2014. "A Single Oncogenic Enhancer Rearrangement Causes Concomitant EVI1 and GATA2 Deregulation in Leukemia." *Cell* 157 (2): 369–81.

Hnisz, Denes, Krishna Shrinivas, Richard A. Young, Arup K. Chakraborty, and Phillip A. Sharp. 2017. "A Phase Separation Model for Transcriptional Control." *Cell* 169 (1): 13–23.

Hsieh, Tsung-Han S., Claudia Cattoglio, Elena Slobodyanyuk, Anders S. Hansen, Xavier Darzacq, and Robert Tjian. 2021. "Enhancer-Promoter Interactions and Transcription Are Maintained upon Acute Loss of CTCF, Cohesin, WAPL, and YY1." *BioRxiv*. https://doi.org/10.1101/2021.07.14.452365.

Hua, Peng, Mohsin Badat, Lars L. P. Hanssen, Lance D. Hentges, Nicholas Crump, Damien J. Downes, Danuta M. Jeziorska, et al. 2021. "Defining Genome Architecture at Base-Pair Resolution." *Nature* 595 (7865): 125–29.

Hughes, Jim R., Nigel Roberts, Simon McGowan, Deborah Hay, Eleni Giannoulatou, Magnus Lynch, Marco De Gobbi, Stephen Taylor, Richard Gibbons, and Douglas R. Higgs. 2014. "Analysis of Hundreds of Cis-Regulatory Landscapes at High Resolution in a Single, High-Throughput Experiment." *Nature Genetics* 46 (2): 205–12.

Ibn-Salem, Jonas, Sebastian Köhler, Michael I. Love, Ho-Ryun Chung, Ni Huang, Matthew E. Hurles, Melissa Haendel, et al. 2014. "Deletions of Chromosomal Regulatory Boundaries Are Associated with Congenital Disease." *Genome Biology* 15 (9): 423.

Javierre, Biola M., Oliver S. Burren, Steven P. Wilder, Roman Kreuzhuber, Steven M. Hill, Sven Sewitz, Jonathan Cairns, et al. 2016. "Lineage-Specific Genome Architecture Links Enhancers and Non-Coding Disease Variants to Target Gene Promoters." *Cell* 167 (5): 1369-1384.e19.

Jin, Fulai, Yan Li, Jesse R. Dixon, Siddarth Selvaraj, Zhen Ye, Ah Young Lee, Chia-An Yen, Anthony D. Schmitt, Celso A. Espinoza, and Bing Ren. 2013. "A High-Resolution Map of the Three-Dimensional Chromatin Interactome in Human Cells." *Nature* 503 (7475): 290–94.

Juven-Gershon, Tamar, and James T. Kadonaga. 2010. "Regulation of Gene Expression via the Core Promoter and the Basal Transcriptional Machinery." *Developmental Biology* 339 (2): 225–29.

Kragesteen, Bjørt K., Malte Spielmann, Christina Paliou, Verena Heinrich, Robert Schöpflin, Andrea Esposito, Carlo Annunziatella, et al. 2018. "Dynamic 3D Chromatin Architecture Contributes to Enhancer Specificity and Limb Morphogenesis." *Nature Genetics* 50 (10): 1463–73.

Kubo, Naoki, Haruhiko Ishii, Xiong Xiong, Simona Bianco, Franz Meitinger, Rong Hu, James D. Hocker, et al. 2021. "Promoter-Proximal CTCF Binding Promotes Distal Enhancer-Dependent Gene Activation." *Nature Structural & Molecular Biology* 28 (2): 152–61.

Kvon, Evgeny Z. 2015. "Using Transgenic Reporter Assays to Functionally Characterize Enhancers in Animals." *Genomics* 106 (3): 185–92.

Kvon, Evgeny Z., Olga K. Kamneva, Uirá S. Melo, Iros Barozzi, Marco Osterwalder, Brandon J. Mannion, Virginie Tissières, et al. 2016. "Progressive Loss of Function in a Limb Enhancer during Snake Evolution." *Cell* 167 (3): 633-642.e11.

Kvon, Evgeny Z., Tomas Kazmar, Gerald Stampfel, J. Omar Yáñez-Cuna, Michaela Pagani, Katharina Schernhuber, Barry J. Dickson, and Alexander Stark. 2014. "Genome-Scale Functional Characterization of Drosophila Developmental Enhancers in Vivo." *Nature* 512 (7512): 91–95.

Kvon, Evgeny Z., Rachel Waymack, Mario Gad, and Zeba Wunderlich. 2021. "Enhancer Redundancy in Development and Disease." *Nature Reviews. Genetics* 22 (5): 324–36.

Kvon, Evgeny Z., Yiwen Zhu, Guy Kelman, Catherine S. Novak, Ingrid Plajzer-Frick, Momoe Kato, Tyler H. Garvin, et al. 2020. "Comprehensive In Vivo Interrogation Reveals Phenotypic Impact of Human Enhancer Variants." *Cell* 180 (6): 1262-1271.e15.

Lettice, Laura A., Sarah Daniels, Elizabeth Sweeney, Shanmugasundaram Venkataraman, Paul S. Devenney, Philippe Gautier, Harris Morrison, Judy Fantes, Robert E. Hill, and David R. FitzPatrick. 2011. "Enhancer-Adoption as a Mechanism of Human Developmental Disease." *Human Mutation* 32 (12): 1492–99.

Lettice, Laura A., Simon J. H. Heaney, Lorna A. Purdie, Li Li, Philippe de Beer, Ben A. Oostra, Debbie Goode, Greg Elgar, Robert E. Hill, and Esther de Graaff. 2003. "A Long-Range Shh Enhancer

Regulates Expression in the Developing Limb and Fin and Is Associated with Preaxial Polydactyly." *Human Molecular Genetics* 12 (14): 1725–35.

Lettice, Laura A., Taizo Horikoshi, Simon J. H. Heaney, Marijke J. van Baren, Herma C. van der Linde, Guido J. Breedveld, Marijke Joosse, et al. 2002. "Disruption of a Long-Range Cis-Acting Regulator for Shh Causes Preaxial Polydactyly." *Proceedings of the National Academy of Sciences of the United States of America* 99 (11): 7548–53.

Li, Guoliang, Xiaoan Ruan, Raymond K. Auerbach, Kuljeet Singh Sandhu, Meizhen Zheng, Ping Wang, Huay Mei Poh, et al. 2012. "Extensive Promoter-Centered Chromatin Interactions Provide a Topological Basis for Transcription Regulation." *Cell* 148 (1–2): 84–98.

Lieberman-Aiden, Erez, Nynke L. van Berkum, Louise Williams, Maxim Imakaev, Tobias Ragoczy, Agnes Telling, Ido Amit, et al. 2009. "Comprehensive Mapping of Long-Range Interactions Reveals Folding Principles of the Human Genome." *Science* 326 (5950): 289–93.

Lonfat, Nicolas, Thomas Montavon, Fabrice Darbellay, Sandra Gitto, and Denis Duboule. 2014. "Convergent Evolution of Complex Regulatory Landscapes and Pleiotropy at Hox Loci." *Science* 346 (6212): 1004–6.

Long, Hannah K., Marco Osterwalder, Ian C. Welsh, Karissa Hansen, James O. J. Davies, Yiran E. Liu, Mervenaz Koska, et al. 2020. "Loss of Extreme Long-Range Enhancers in Human Neural Crest Drives a Craniofacial Disorder." *Cell Stem Cell* 27 (5): 765-783.e14.

Long, Hannah K., Sara L. Prescott, and Joanna Wysocka. 2016. "Ever-Changing Landscapes: Transcriptional Enhancers in Development and Evolution." *Cell* 167 (5): 1170–87.

Love, Michael I., Wolfgang Huber, and Simon Anders. 2014. "Moderated Estimation of Fold Change and Dispersion for RNA-Seq Data with DESeq2." *Genome Biology* 15 (12): 550.

Lupiáñez, Darío G., Katerina Kraft, Verena Heinrich, Peter Krawitz, Francesco Brancati, Eva Klopocki, Denise Horn, et al. 2015. "Disruptions of Topological Chromatin Domains Cause Pathogenic Rewiring of Gene-Enhancer Interactions." *Cell* 161 (5): 1012–25.

Madsen, Jesper G. S., Maria S. Madsen, Alexander Rauch, Sofie Traynor, Elvira L. Van Hauwaert, Anders K. Haakonsson, Biola M. Javierre, Mette Hyldahl, Peter Fraser, and Susanne Mandrup. 2020. "Highly Interconnected Enhancer Communities Control Lineage-Determining Genes in Human Mesenchymal Stem Cells." *Nature Genetics* 52 (11): 1227–38.

Mannion, Brandon J., Marco Osterwalder, Stella Tran, Ingrid Plajzer-Frick, Catherine S. Novak, Veena Afzal, Jennifer A. Akiyama, et al. 2022. "Uncovering Hidden Enhancers Through Unbiased In Vivo Testing." *BioRxiv*. https://doi.org/10.1101/2022.05.29.493901.

Martinez-Ara, Miguel, Federico Comoglio, Joris van Arensbergen, and Bas van Steensel. 2022. "Systematic Analysis of Intrinsic Enhancer-Promoter Compatibility in the Mouse Genome." *Molecular Cell* 82 (13): 2519-2531.e6.

Mateo, Leslie J., Sedona E. Murphy, Antonina Hafner, Isaac S. Cinquini, Carly A. Walker, and Alistair N. Boettiger. 2019. "Visualizing DNA Folding and RNA in Embryos at Single-Cell Resolution." *Nature* 568 (7750): 49–54.

Mifsud, Borbala, Filipe Tavares-Cadete, Alice N. Young, Robert Sugar, Stefan Schoenfelder, Lauren Ferreira, Steven W. Wingett, et al. 2015. "Mapping Long-Range Promoter Contacts in Human Cells with High-Resolution Capture Hi-C." *Nature Genetics* 47 (6): 598–606.

Montavon, Thomas, Natalia Soshnikova, Bénédicte Mascrez, Elisabeth Joye, Laurie Thevenet, Erik Splinter, Wouter de Laat, François Spitz, and Denis Duboule. 2011. "A Regulatory Archipelago Controls Hox Genes Transcription in Digits." *Cell* 147 (5): 1132–45.

Morgan, Stefanie L., Natasha C. Mariano, Abel Bermudez, Nicole L. Arruda, Fangting Wu, Yunhai Luo, Gautam Shankar, et al. 2017. "Manipulation of Nuclear Architecture through CRISPR-Mediated Chromosomal Looping." *Nature Communications* 8 (July): 15993.

Nora, Elphège P., Bryan R. Lajoie, Edda G. Schulz, Luca Giorgetti, Ikuhiro Okamoto, Nicolas Servant, Tristan Piolot, et al. 2012. "Spatial Partitioning of the Regulatory Landscape of the X-Inactivation Centre." *Nature* 485 (7398): 381–85.

Northcott, Paul A., Catherine Lee, Thomas Zichner, Adrian M. Stütz, Serap Erkek, Daisuke Kawauchi, David J. H. Shih, et al. 2014. "Enhancer Hijacking Activates GFI1 Family Oncogenes in Medulloblastoma." *Nature* 511 (7510): 428–34.

Orlando, Giulia, Ben Kinnersley, and Richard S. Houlston. 2018. "Capture Hi-C Library Generation and Analysis to Detect Chromatin Interactions." *Current Protocols in Human Genetics / Editorial Board, Jonathan L. Haines ... [et Al.]*, July, e63.

Osterwalder, Marco, Iros Barozzi, Virginie Tissières, Yoko Fukuda-Yuzawa, Brandon J. Mannion, Sarah Y. Afzal, Elizabeth A. Lee, et al. 2018. "Enhancer Redundancy Provides Phenotypic Robustness in Mammalian Development." *Nature* 554 (7691): 239–43.

Osterwalder, Marco, Stella Tran, Riana D. Hunter, Eman M. Meky, Kianna von Maydell, Anne N. Harrington, Janeth Godoy, et al. 2022. "Characterization of Mammalian In Vivo Enhancers Using Mouse Transgenesis and CRISPR Genome Editing." *Methods in Molecular Biology* 2403: 147–86.

Oudelaar, A. Marieke, and Douglas R. Higgs. 2021. "The Relationship between Genome Structure and Function." *Nature Reviews. Genetics* 22 (3): 154–68.

Pachano, Tomas, Víctor Sánchez-Gaya, Thais Ealo, Maria Mariner-Faulí, Tore Bleckwehl, Helena G. Asenjo, Patricia Respuela, et al. 2021. "Orphan CpG Islands Amplify Poised Enhancer Regulatory Activity and Determine Target Gene Responsiveness." *Nature Genetics* 53 (7): 1036–49.

Padhi, Evin M., Tristan J. Hayeck, Zhang Cheng, Sumantra Chatterjee, Brandon J. Mannion, Marta Byrska-Bishop, Marjolaine Willems, et al. 2021. "Coding and Noncoding Variants in EBF3 Are Involved in HADDS and Simplex Autism." *Human Genomics* 15 (1): 44.

Paliou, Christina, Philine Guckelberger, Robert Schöpflin, Verena Heinrich, Andrea Esposito, Andrea M. Chiariello, Simona Bianco, et al. 2019. "Preformed Chromatin Topology Assists Transcriptional Robustness of Shh during Limb Development." *Proceedings of the National Academy of Sciences of the United States of America* 116 (25): 12390–99.

Pattabiraman, Kartik, Olga Golonzhka, Susan Lindtner, Alex S. Nord, Leila Taher, Renee Hoch, Shanni N. Silberberg, et al. 2014. "Transcriptional Regulation of Enhancers Active in Protodomains of the Developing Cerebral Cortex." *Neuron* 82 (5): 989–1003.

Pennacchio, Len A., Nadav Ahituv, Alan M. Moses, Shyam Prabhakar, Marcelo A. Nobrega, Malak Shoukry, Simon Minovitsky, et al. 2006. "In Vivo Enhancer Analysis of Human Conserved Non-Coding Sequences." *Nature* 444 (7118): 499–502.

Perry, Michael W., Alistair N. Boettiger, Jacques P. Bothma, and Michael Levine. 2010. "Shadow Enhancers Foster Robustness of Drosophila Gastrulation." *Current Biology: CB* 20 (17): 1562–67.

Platt, James L., Rafik Salama, James Smythies, Hani Choudhry, James O. J. Davies, Jim R. Hughes, Peter J. Ratcliffe, and David R. Mole. 2016. "Capture‐C Reveals Preformed Chromatin Interactions between HIF‐binding Sites and Distant Promoters." *EMBO Reports* 17 (10): 1410–21.

Putri, Givanna H., Simon Anders, Paul Theodor Pyl, John E. Pimanda, and Fabio Zanini. 2022. "Analysing High-Throughput Sequencing Data in Python with HTSeq 2.0." *Bioinformatics* , March. https://doi.org/10.1093/bioinformatics/btac166.

Rao, Suhas S. P., Miriam H. Huntley, Neva C. Durand, Elena K. Stamenova, Ivan D. Bochkov, James T. Robinson, Adrian L. Sanborn, et al. 2014. "A 3D Map of the Human Genome at Kilobase Resolution Reveals Principles of Chromatin Looping." *Cell* 159 (7): 1665–80.

Ringel, Alessa R., Quentin Szabo, Andrea M. Chiariello, Konrad Chudzik, Robert Schöpflin, Patricia Rothe, Alexandra L. Mattei, et al. 2022. "Repression and 3D-Restructuring Resolves Regulatory Conflicts in Evolutionarily Rearranged Genomes." *Cell* 185 (20): 3689-3704.e21.

Robson, Michael I., Alessa R. Ringel, and Stefan Mundlos. 2019. "Regulatory Landscaping: How Enhancer-Promoter Communication Is Sculpted in 3D." *Molecular Cell* 74 (6): 1110–22.

Rodríguez-Carballo, Eddie, Lucille Lopez-Delisle, Andréa Willemin, Leonardo Beccari, Sandra Gitto, Bénédicte Mascrez, and Denis Duboule. 2020. "Chromatin Topology and the Timing of Enhancer Function at the HoxD Locus." *Proceedings of the National Academy of Sciences of the United States of America* 117 (49): 31231–41.

Rodríguez-Carballo, Eddie, Lucille Lopez-Delisle, Ye Zhan, Pierre J. Fabre, Leonardo Beccari, Imane El-Idrissi, Thi Hanh Nguyen Huynh, Hakan Ozadam, Job Dekker, and Denis Duboule. 2017. "The HoxD Cluster Is a Dynamic and Resilient TAD Boundary Controlling the Segregation of Antagonistic Regulatory Landscapes." *Genes & Development* 31 (22): 2264–81.

Rubin, Adam J., Brook C. Barajas, Mayra Furlan-Magaril, Vanessa Lopez-Pajares, Maxwell R. Mumbach, Imani Howard, Daniel S. Kim, et al. 2017. "Lineage-Specific Dynamic and Pre-Established Enhancer–Promoter Contacts Cooperate in Terminal Differentiation." *Nature Genetics* 49 (10): 1522–28.

Sagai, Tomoko, Masaki Hosoya, Youichi Mizushina, Masaru Tamura, and Toshihiko Shiroishi. 2005. "Elimination of a Long-Range Cis-Regulatory Module Causes Complete Loss of Limb-Specific Shh Expression and Truncation of the Mouse Limb." *Development* 132 (4): 797–803.

Schoenfelder, Stefan, and Peter Fraser. 2019a. "Long-Range Enhancer–Promoter Contacts in Gene Expression Control." *Nature Reviews. Genetics* 20 (8): 437–55.

———. 2019b. "Long-Range Enhancer-Promoter Contacts in Gene Expression Control." *Nature Reviews. Genetics* 20 (8): 437–55.

Schoenfelder, Stefan, Mayra Furlan-Magaril, Borbala Mifsud, Filipe Tavares-Cadete, Robert Sugar, Biola-Maria Javierre, Takashi Nagano, et al. 2015. "The Pluripotent Regulatory Circuitry Connecting Promoters to Their Long-Range Interacting Elements." *Genome Research* 25 (4): 582–97.

Serebreni, Leonid, and Alexander Stark. 2021. "Insights into Gene Regulation: From Regulatory Genomic Elements to DNA-Protein and Protein-Protein Interactions." *Current Opinion in Cell Biology* 70 (June): 58–66.

Shibata, Mikihito, Hiromi Nakao, Hiroshi Kiyonari, Takaya Abe, and Shinichi Aizawa. 2011. "MicroRNA-9 Regulates Neurogenesis in Mouse Telencephalon by Targeting Multiple Transcription Factors." *The Journal of Neuroscience: The Official Journal of the Society for Neuroscience* 31 (9): 3407–22.

Shlyueva, Daria, Gerald Stampfel, and Alexander Stark. 2014. "Transcriptional Enhancers: From Properties to Genome-Wide Predictions." *Nature Reviews. Genetics* 15 (4): 272–86.

Short, Patrick J., Jeremy F. McRae, Giuseppe Gallone, Alejandro Sifrim, Hyejung Won, Daniel H. Geschwind, Caroline F. Wright, et al. 2018. "De Novo Mutations in Regulatory Elements in Neurodevelopmental Disorders." *Nature* 555 (7698): 611–16.

Siersbæk, Rasmus, Jesper Grud Skat Madsen, Biola Maria Javierre, Ronni Nielsen, Emilie Kristine Bagge, Jonathan Cairns, Steven William Wingett, et al. 2017. "Dynamic Rewiring of Promoter-Anchored Chromatin Loops during Adipocyte Differentiation." *Molecular Cell* 66 (3): 420-435.e5.

Simmons, Elizabeth, Roshan Vaid, Xin Yang Bing, Michael Levine, Mattias Mannervik, and Juan M. Vaquerizas. 2021. "Independence of Chromatin Conformation and Gene Regulation during Drosophila Dorsoventral Patterning." *Nature Genetics* 53 (4): 487–99.

Smemo, Scott, Juan J. Tena, Kyoung-Han Kim, Eric R. Gamazon, Noboru J. Sakabe, Carlos Gómez-Marín, Ivy Aneas, et al. 2014. "Obesity-Associated Variants within FTO Form Long-Range Functional Connections with IRX3." *Nature* 507 (7492): 371–75.

Smith, Constance M., Jacqueline H. Finger, Terry F. Hayamizu, Ingeborg J. McCright, Jingxia Xu, Joanne Berghout, Jeff Campbell, et al. 2014. "The Mouse Gene Expression Database (GXD): 2014 Update." *Nucleic Acids Research* 42 (Database issue): D818-24.

Snetkova, Valentina, Athena R. Ypsilanti, Jennifer A. Akiyama, Brandon J. Mannion, Ingrid Plajzer-Frick, Catherine S. Novak, Anne N. Harrington, et al. 2021. "Ultraconserved Enhancer Function Does Not Require Perfect Sequence Conservation." *Nature Genetics* 53 (4): 521–28.

Tan, Siok-Lay, Toshiyuki Ohtsuka, Aitor González, and Ryoichiro Kageyama. 2012. "MicroRNA9 Regulates Neural Stem Cell Differentiation by Controlling Hes1 Expression Dynamics in the Developing Brain." *Genes to Cells: Devoted to Molecular & Cellular Mechanisms* 17 (12): 952–61.

Tolhuis, Bas, Robert Jan Palstra, Erik Splinter, Frank Grosveld, and Wouter de Laat. 2002. "Looping and Interaction between Hypersensitive Sites in the Active Beta-Globin Locus." *Molecular Cell* 10 (6): 1453–65.

Tsai, Albert, Mariana Rp Alves, and Justin Crocker. 2019. "Multi-Enhancer Transcriptional Hubs Confer Phenotypic Robustness." *ELife* 8 (July). https://doi.org/10.7554/eLife.45325.

Turner, Tychele N., Bradley P. Coe, Diane E. Dickel, Kendra Hoekzema, Bradley J. Nelson, Michael C. Zody, Zev N. Kronenberg, et al. 2017. "Genomic Patterns of De Novo Mutation in Simplex Autism." *Cell* 171 (3): 710-722.e12.

Uslu, Veli Vural, Massimo Petretich, Sandra Ruf, Katja Langenfeld, Nuno A. Fonseca, John C. Marioni, and François Spitz. 2014. "Long-Range Enhancers Regulating Myc Expression Are Required for Normal Facial Morphogenesis." *Nature Genetics* 46 (7): 753–58.

Visel, Axel, Simon Minovitsky, Inna Dubchak, and Len A. Pennacchio. 2006. "VISTA Enhancer Browser—a Database of Tissue-Specific Human Enhancers." *Nucleic Acids Research* 35 (suppl_1): D88–92.

Visel, Axel, Edward M. Rubin, and Len A. Pennacchio. 2009. "Genomic Views of Distant-Acting Enhancers." *Nature* 461 (7261): 199–205.

Visel, Axel, Yiwen Zhu, Dalit May, Veena Afzal, Elaine Gong, Catia Attanasio, Matthew J. Blow, Jonathan C. Cohen, Edward M. Rubin, and Len A. Pennacchio. 2010. "Targeted Deletion of the 9p21 Non-Coding Coronary Artery Disease Risk Interval in Mice." *Nature* 464 (7287): 409–12.

Visser, Mijke, Manfred Kayser, and Robert-Jan Palstra. 2012. "HERC2 Rs12913832 Modulates Human Pigmentation by Attenuating Chromatin-Loop Formation between a Long-Range Enhancer and the OCA2 Promoter." *Genome Research* 22 (3): 446–55.

Williamson, Iain, Laura A. Lettice, Robert E. Hill, and Wendy A. Bickmore. 2016. "Shh and ZRS Enhancer Colocalisation Is Specific to the Zone of Polarising Activity." *Development* 143 (16): 2994–3001.

Wingett, Steven, Philip Ewels, Mayra Furlan-Magaril, Takashi Nagano, Stefan Schoenfelder, Peter Fraser, and Simon Andrews. 2015. "HiCUP: Pipeline for Mapping and Processing Hi-C Data." *F1000Research* 4 (November): 1310.

Wunderlich, Zeba, Meghan D. J. Bragdon, Ben J. Vincent, Jonathan A. White, Javier Estrada, and Angela H. DePace. 2016. "Krüppel Expression Levels Are Maintained through Compensatory Evolution of Shadow Enhancers." *Cell Reports* 14 (12): 3030.

Xiao, Jordan Yupeng, Antonina Hafner, and Alistair N. Boettiger. 2021. "How Subtle Changes in 3D Structure Can Create Large Changes in Transcription." *ELife* 10 (July). https://doi.org/10.7554/eLife.64320.

Yanchus, Connor, Kristen L. Drucker, Thomas M. Kollmeyer, Ricky Tsai, Warren Winick-Ng, Minggao Liang, Ahmad Malik, et al. 2022. "A Noncoding Single-Nucleotide Polymorphism at 8q24 Drives *IDH1*-Mutant Glioma Formation." *Science* 378 (6615): 68–78.

Yang, Yali, Mingxin Ren, Chao Song, Dan Li, Shahid Hussain Soomro, Yajie Xiong, Hongfeng Zhang, and Hui Fu. 2017. "LINC00461, a Long Non-Coding RNA, Is Important for the Proliferation and Migration of Glioma Cells." *Oncotarget* 8 (48): 84123–39.

Yoo, Andrew S., Alfred X. Sun, Li Li, Aleksandr Shcheglovitov, Thomas Portmann, Yulong Li, Chris Lee-Messer, Ricardo E. Dolmetsch, Richard W. Tsien, and Gerald R. Crabtree. 2011. "MicroRNA-Mediated Conversion of Human Fibroblasts to Neurons." *Nature* 476 (7359): 228–31.

Zabidi, Muhammad A., Cosmas D. Arnold, Katharina Schernhuber, Michaela Pagani, Martina Rath, Olga Frank, and Alexander Stark. 2014. "Enhancer–Core-Promoter Specificity Separates Developmental and Housekeeping Gene Regulation." *Nature* 518 (7540): 556–59.

Zerbino, Daniel R., Steven P. Wilder, Nathan Johnson, Thomas Juettemann, and Paul R. Flicek. 2015. "The Ensembl Regulatory Build." *Genome Biology* 16 (March): 56.

Zhao, Chunnian, Guoqiang Sun, Shengxiu Li, and Yanhong Shi. 2009. "A Feedback Regulatory Loop Involving MicroRNA-9 and Nuclear Receptor TLX in Neural Stem Cell Fate Determination." *Nature Structural & Molecular Biology* 16 (4): 365–71.

Zuin, Jessica, Gregory Roth, Yinxiu Zhan, Julie Cramard, Josef Redolfi, Ewa Piskadlo, Pia Mach, et al. 2022. "Nonlinear Control of Transcription through Enhancer–Promoter Interactions." *Nature* 604 (7906): 571–77.

Acknowledgments

The authors would like to acknowledge the UCI Transgenic Mouse Facility for help with generation of enhancer knockout mice and the UCI Genomics High Throughput Facility for help with sequencing. **Funding:** This work was supported by National Institutes of Health grants R00HG009682 and DP2GM149555 (to E.Z.K.) and R01HG003988 (to L.A.P.). Z.C. was supported by NSF grant DMS1763272 (to Qing Nie) and Simons Foundation grant 594598 (to Qing Nie). Research conducted at the E.O. Lawrence Berkeley National Laboratory was performed under Department of Energy Contract DE-AC02-05CH11231, University of California. **Author contributions:** E.Z.K. conceived the project with input from Z.C., V.S., D.E.D., A.V. and L.A.P. Z.C., V.S., I.B. and E.Z.K. designed experiments. E.Z.K., Z.C., V.S., G.B., S.J., B.C. performed Capture Hi-C experiments and Z.C. analyzed the data with input from E.Z.K. E.Z.K. and Z.C. performed the enhancer knockout studies and Z.C. analyzed the data. A.A.C. and J.L.R performed ISH experiments. E.Z.K and Z.C wrote the manuscript with input from the remaining authors. **Competing interests:** The

authors declare no competing interests. **Data and materials availability:** All sequencing data is available at GEO: GSE217078.

Materials and Methods

Tissue collection

All animal work was reviewed and approved by the Lawrence Berkeley National Laboratory Animal Welfare and Research Committee and the University Laboratory Animal Resources (ULAR). Mouse embryonic tissues, including the forebrain, midbrain, hindbrain, neural tube, tail, facial mesenchyme, forelimb, hindlimb, heart and trunk, were collected from FVB/NCrl strain *Mus musculus* animals (Charles River). Wild-type male and female mice were mated using a standard timed breeding strategy and E11.5 embryos were collected for dissection using approved institutional protocols. Embryos were excluded if they were not at the expected developmental stage. Only one embryonic litter was processed at a time and tissues and embryos were kept on ice to avoid degradation during tissue collection. Tissue from multiple embryos was pooled together in the same collection tube, and at least two separate collection tubes were collected for each tissue for biological replication.

Tissue processing for Hi-C library

To prepare nuclei for constructing the Hi-C library, tissues were incubated with collagenase (Gibco) in a thermomixer at 37 °C until the cells were dissociated, about 10 to 20 min. Cells were fixed by adding formaldehyde (Sigma-Aldrich) to a final concentration of 2% at RT for 10 min as described previously (Paliou et al. 2019; Dryden et al. 2014). Ice-cold glycine solution was added to a final concentration of 200 mM to quench crosslinking. Cells were then resuspended in cold lysis buffer (50 mM Tris, pH 7.5, 150 mM NaCl, 5 mM EDTA, 0.5% NP-40, 1.15% Triton X-100 and 1X protease inhibitor cocktail (Thermo Scientific)) and incubated on ice for 15 min. Pellets of nuclei were obtained by centrifuge at 750 *g* for 5 min at 4 °C, followed by snap-freezing and storage at -80 °C.

Generation of Hi-C library

Hi-C libraries were prepared as described previously (Hughes et al. 2014; Dryden et al. 2014; Orlando, Kinnersley, and Houlston 2018). Briefly, frozen nuclei pellets (2-6 million) were thawed on ice, followed by adding SDS and Triton X-100 to remove non-crosslinked proteins and sequester SDS, and digested using DpnII (NBE) overnight at 37 °C. The ends of restriction fragments were labeled with biotinylated dCTP and ligated at room temperature for 4 hours. After de-crosslinking and precipitation, ligated products were sheared using a Covaris sonicator (duty cycle: 10%, intensity: 5, cycles per burst: 200,

treatment time: 180 s in total) to an average fragment size of 200bp. The ligated sheared 3C libraries (10-12 ug for each replicate) were pulled down using Streptavidin Dynabeads (Thermo Scientific) to get rid of unligated fragments, followed by end repair, adaptor ligation and library amplification according to modified Agilent SureSelectXT protocol.

5 **Capture Hi-C probe design**

To perform ecHi-C, we designed 120-mer RNA probes, targeting 935 enhancer regions that showed highly reproducible activity at E11.5 from VISTA Enhancer Database (Pennacchio et al. 2006) (**Table S1**). We also designed RNA probes targeting 176 promoters and 87 elements with no reproducible enhancer activity at E11.5 as negative controls
10 (**Table S1**). All elements shorter than 2 kb were re-sized to 2 kb (± 1 kb from their central coordinate).

We designed 20,452 120-mer probes (each region was covered by on average 17 RNA probes) using the following pipeline. We first identified the DpnII restriction sites (GATC) overlapping each element by generating a genome-wide map of cut sites using vmatch
15 (http://www.vmatch.de/). For each of the DpnII restriction sites overlapping the re-sized VISTA elements, ± 240 bp around the recognition site were considered for tiling. Among the resulting regions, those found within 60 bp of each other were further merged. After that, these regions were tiled (from -60 bp to +60 bp) using overlapping 120 bp windows, with a step of 60 bp. The tiles obtained were further filtered based on their overlap with

repetitive elements and their predicted mappability using short reads. For filtering based on mappability, the wgEncodeCrgMapabilityAlign36mer.bigWig track from the UCSC genome browser (mm9) was used. Only tiles showing a mappability score of 1 across all 120 bp were retained. For exclusion based on repeats, the tiles were first lifted to mm10 (using liftOver), then each tile showing an overlap of at least 10% with an annotated repeat in the RepeatMasker track of the UCSC genome browser were excluded. Following that, only those overlapping elements represented by at least three tiles were considered for the final design. For capture Hi-C experiments at the *Shh*-ZRS locus (**Fig. 5**) we designed a separate panel that covered the ZRS enhancer, part of the bacterial LacZ sequence and 9 control regions (**Table S1**).

Capture Hi-C library construction and sequencing

The ecHi-C library was created by performing a target-enrichment protocol using capture RNA probes according to Agilent SureSelect XT protocol with an input amount of 750 ng of Hi-C library per sample. Following hybridization to the RNA oligo library, each ecHi-C library was sequenced (paired-end 100 or 150 bp) to enrich enhancer-centric interactions yielding a total of 1 billion unique paired-end reads.

Capture Hi-C data analysis

Ligated reads were trimmed using DpnII restriction recognition sites and mapped to the DpnII-digested reference genome (mm10) using HiCUP (Wingett et al. 2015), followed

by quality filtering and deduplication. For each tissue, the ecHi-C experiment produced, on average, 20 million unique on-target paired-end reads, resulting in a total of 200 million valid read pairs (**Table S1**).

Next, all DpnII fragments overlapping with the same bait region were merged into a single fragment *in silico*. Subsequently, the rest of the DpnII fragments were merged based on the size distribution of the pooled fragments that overlapped with bait regions. The mean fragment size of pooled fragments is ~3,000 bp. Significant interactions were called by CHiCAGO (score > 5) with the default setting (Cairns et al. 2016; Freire-Pritchett et al. 2021) using combined replicates from HiCUP pipeline, by using the design file with the following parameters: --minFragLen=300 --maxFragLen=20000 --binsize=20000 --maxLBrownEst=3000000 --removeAdjacent=FALSE. We removed significant interactions that didn't have valid ditag reads on neighboring fragments to avoid spurious interaction spikes (Schoenfelder et al. 2015). Interactions called >2 Mb from the bait regions were excluded from the downstream analysis.

To compare interaction frequencies between different tissues, read counts were normalized across 10 tissues by Chicdiff (Cairns et al. 2019; Freire-Pritchett et al. 2021) to account for library size and background differences between samples. We used the output from CHiCAGO to make a peak matrix and performed the normalization in Chicdiff with the following setting parameters: norm="fullmean", score=3, RUexpand=3L.

For the visualization of interactions on a heatmap, we performed further normalization by scaling the sum of normalized read depth around 10 kb from the midpoint of bait regions for each bait across 10 tissues.

For the classification of enhancer-interacting regions in **Fig. S1D**, we used promoter annotations from the latest version of Ensembl Regulatory Build (Zerbino et al. 2015), CTCF binding sites at E12.5 from publicly available data (GSE181383) (Amândio et al. 2021), putative enhancers based on H3K27ac occupancy (from E10.5 to E12.5) and polycomb associated H3K27me3 marked regions (at E10.5 to E12.5) from the ENCODE database (ENCODE Project Consortium et al. 2020). We further filtered promoters by only keeping those within ±2.5 kb around TSSs that were transcribed (TPM > 0.5 from RNA-seq data in ENCODE database) in at least one of the following embryonic stages: E10.5, E11.5 and E12.5. CTCF sites were divided into two categories based on whether they were within a TAD or at a TAD boundary. Overlap of interaction peaks with promoters, CTCF sites, enhancers and polycomb regions were computed sequentially, which means peaks were assigned to only one category, and by extending the interaction peaks by ±5 kb.

For the E–P interaction analysis in **Fig. 4** and **S5, S7**, we focused on 919 E–P interactions in which the enhancer and interacting gene are both active in at least one tissue. *In vivo*

enhancer strength used in **Fig. 4** and **S5** is based on a metric that considers both the reproducibility and strength of the enhancer in LacZ reporter assay.

To perform *k*-means clustering for E–P interactions in **Fig. 4A**, normalized interaction frequencies were scaled to the max value among 10 tissues, and clustering was performed in R with k = 10 and nstart=30. Clusters were ordered using hclust() with the "ward.D" method.

For DNA methylation and DNase signal comparison for interacting and skipped genes in **Fig. 2 and S3**, we counted the read counts ±1 kb around the TSS of each gene for every enhancer-gene interaction. For comparison to H3K27me3 and H3K9me3 regions, we extended the region analyzed to ±2.5 kb of sequence around the TSS of each gene. The differences between interacting and skipped genes were calculated by nonparametric Wilcoxon–Mann–Whitney tests.

For E–E interaction analysis in **Fig. 4 and S8**, we only considered interactions that target fragments overlapping with H3K27ac peaks in E11.5 embryos (signal >5).

Generation of enhancer knockout and knockin mice

Enhancer knockout mice were created using a modified CRISPR/Cas9 protocol as described previously (Osterwalder et al. 2022, 2018). Briefly, pronuclei of FVB mouse zygotes were injected with a mix of Cas9 protein (final concentration of 20 ng/ul, IDT)

and sgRNAs targeting enhancer regions (50 ng/ul) (**Fig. S4**). To replace the ZRS with the fragment of the LacZ sequence, we used a previously described strategy (Kvon et al. 2016). Briefly, pronuclei of FVB mouse zygotes were injected with a donor plasmid (25 ng/ul) containing LacZ sequence and homology arms from the ZRS region, sgRNA targeting the
5 ZRS locus and Cas9 protein (Kvon et al. 2016) (**Fig. S9**). F_0 mice were genotyped by PCR and Sanger sequencing using the following primers:

Primer name	Sequence (5′-3′)
hs654-F1	AGGTTCTGGCAAGTGTAAGCAA
hs654-R1	AGCCCTGTCTCAAACCCCTCCC
hs654-F2	TTGCATGGGGCCTCAATGACCC
hs654-R2	TGGCAGGGAGGGGAGGGAAAAG
hs267-853-F1	ATTCTGGCCAGTTGCATGCTGT
hs267-853-R1	TGACACTGGAAAGCCTACCAACA
hs267-853-R2	CACAGGGCTGGGCTCCAACATG
LacZ-F1	GGTAGAGGCCAGGAAGTCG
LacZ-R1	GACGTGTCAGTAGTCGCTCAGA
LacZ-F2	ATCAGATGTTCTGTGTACGTGACC
LacZ-R2	GTCATTTCAACTTTCTTATTTCAGTATA

In situ hybridization

The *Shh* transcript distribution in E10.5 mouse embryonic limb buds was assessed by whole mount *in situ* hybridization using digoxigenin-labeled antisense riboprobes as previously described (Kvon et al. 2016).

RNA-seq data generation and analysis

Dissected tissues were immediately submerged in RNAprotect Tissue Reagent (Qiagen) and stored at -80 ℃. Multiple samples from the same tissue and genotype were pooled into at least 1 million cells for each of the two replicates. RNA isolation, preparation of RNA library and transcriptome sequencing was conducted by Novogene Co., LTD (Beijing, China). All RNA-seq experiments were performed in 2 biological duplicates. Paired-end reads were mapped to the reference genome (mm10) using STAR software with default parameters (Dobin et al. 2013) and were counted on RefSeq genes by HTSeq (Putri et al. 2022). Differential gene expression analysis was performed using DEseq2 (Love, Huber, and Anders 2014). Genes with adjusted p-value < 0.05 were considered differentially expressed.

Statistics

For statistics that compare the interaction frequencies, histone modifications, or DNase accessibility, no assumptions of normality were made, but rather all tests were performed using nonparametric Wilcoxon–Mann–Whitney tests or nonparametric Fisher's exact

tests. Wilcoxon–Mann–Whitney tests were performed in R using the wilcox.test() performed as a two-sided test.

Data Accessibility

Sequencing data are available at the Gene Expression Omnibus repository with the accession number GSE217078.

Supplementary Figures

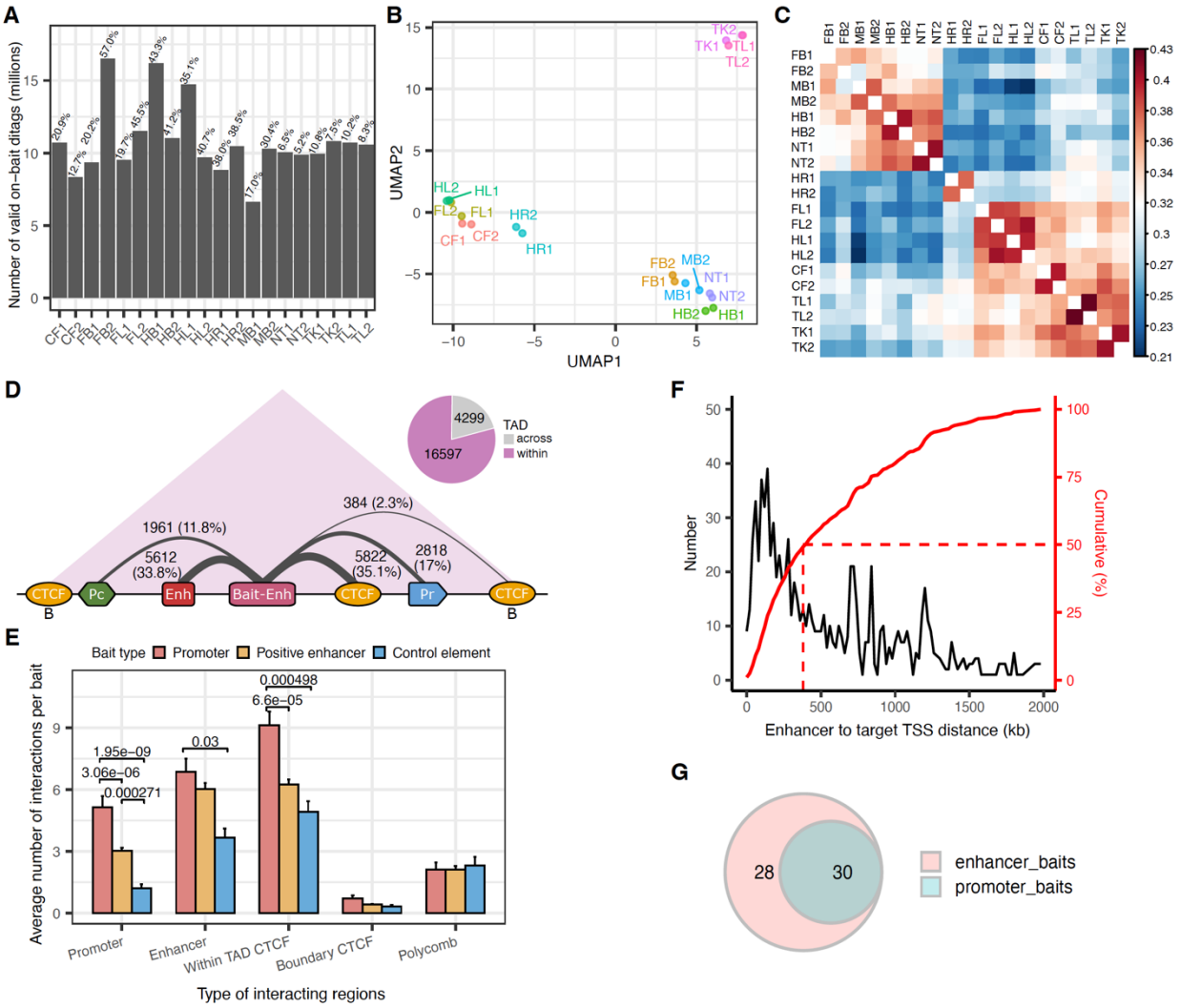

Supplementary Figure 1: EcHi-C identifies enhancer-centric chromatin interactions. (**A**) On-target read counts for each library. FB, forebrain. MB, midbrain. HB, hindbrain. CF, craniofacial mesenchyme. HR, heart. FL, forelimb. HL, hindlimb. TK, trunk. TL, tail. NT, neural tube. The number on each bar denotes the percentage of on-target reads out of total valid ditags in each library. (**B, C**) Principal component analysis and hierarchical clustering of all replicates based on the presence of peaks called by CHiCAGO in each replicate (considering peaks with valid ditags on neighboring fragments). (**D**) Significant enhancer-centric chromatin interactions identified in this study. The number on each link represents the number of fragments falling into different annotation categories and the width of links is proportional to the percentage (in the parentheses) of different kinds of interactions. Only interactions within 2 Mb are included. CTCF sites with "B": CTCF sites at TAD boundary; Pc: polycomb; Enh: enhancers; Bait-Enh: baited enhancers; Pr: promoters. (**E**) An average number of interactions detected per bait for different kinds of baits (promoter, enhancer and control harmful elements). *P* values were calculated by a two-sided Wilcox test and adjusted for multiple testing. (**F**) Distribution of genomic distances between enhancers and the TSSs of interacting genes (black, frequencies; red, cumulative). (**G**) Venn diagram shows the overlap between significant interactions called from enhancer baits and corresponding promoter baits.

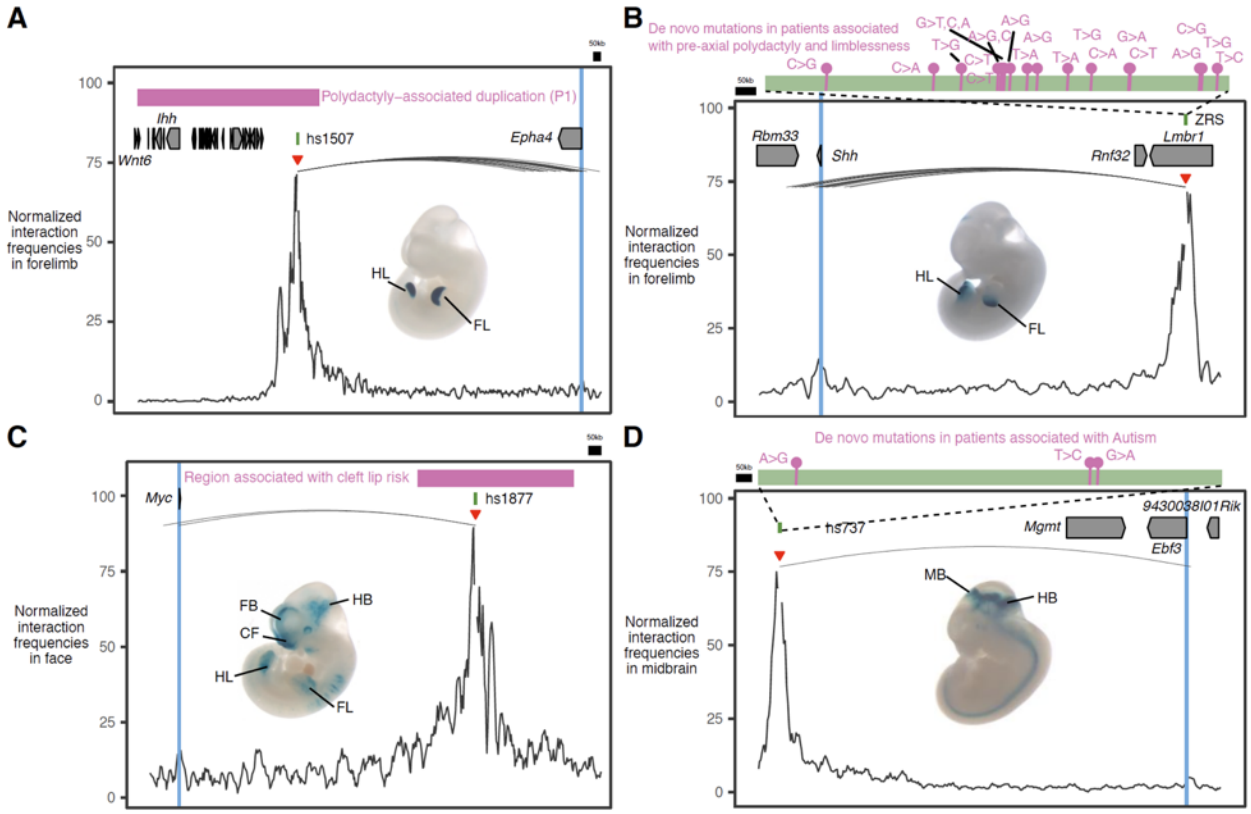

Supplementary Fig 2: Examples of enhancer—promoter interactions linked to congenital disorders. (**A**) Hs1507 limb enhancer located in the non-coding region is duplicated in patients with polydactyly (pink box indicates the homologous region in the mouse genome) (Lupiáñez et al. 2015). Hs1507 forms significant chromatin interactions with the promoter of the *Epha4* located ~1.5 Mb away. Shown is the *Epha4* genomic region (chr1:74,788,119-77,634,678; mm10). (**B**) Many *de novo* rare variants identified in patients with preaxial polydactyly (Kvon et al. 2020) are located in the ZRS limb enhancer which forms significant interactions with the promoter of *Shh* located ~850 kb away. The *Shh* genomic region (chr5:28,320,000-29,400,000; mm10). (**C**) Hs1877 face enhancer located in the non-coding region is associated with 146 SNPs in patients with cleft lip risk (Uslu et al. 2014) (pink box indicates the homologous region in the mouse genome). Hs1877 forms significant chromatin interactions with the promoter of the *Myc* located ~900 kb away in the face. The *Myc* genomic region (chr15:61,880,003-63,506,895; mm10). (**D**) Three de novo rare variants identified in patients with limb malformation are located in the hs737 midbrain/hindbrain enhancer (Padhi et al. 2021; Turner et al. 2017), which forms strong significant interactions with the promoter of *Ebf3* located ~1,000 kb away in the midbrain. Shown is the Ebf3 genomic region (chr7:136,018,204-137,420,338; mm10).

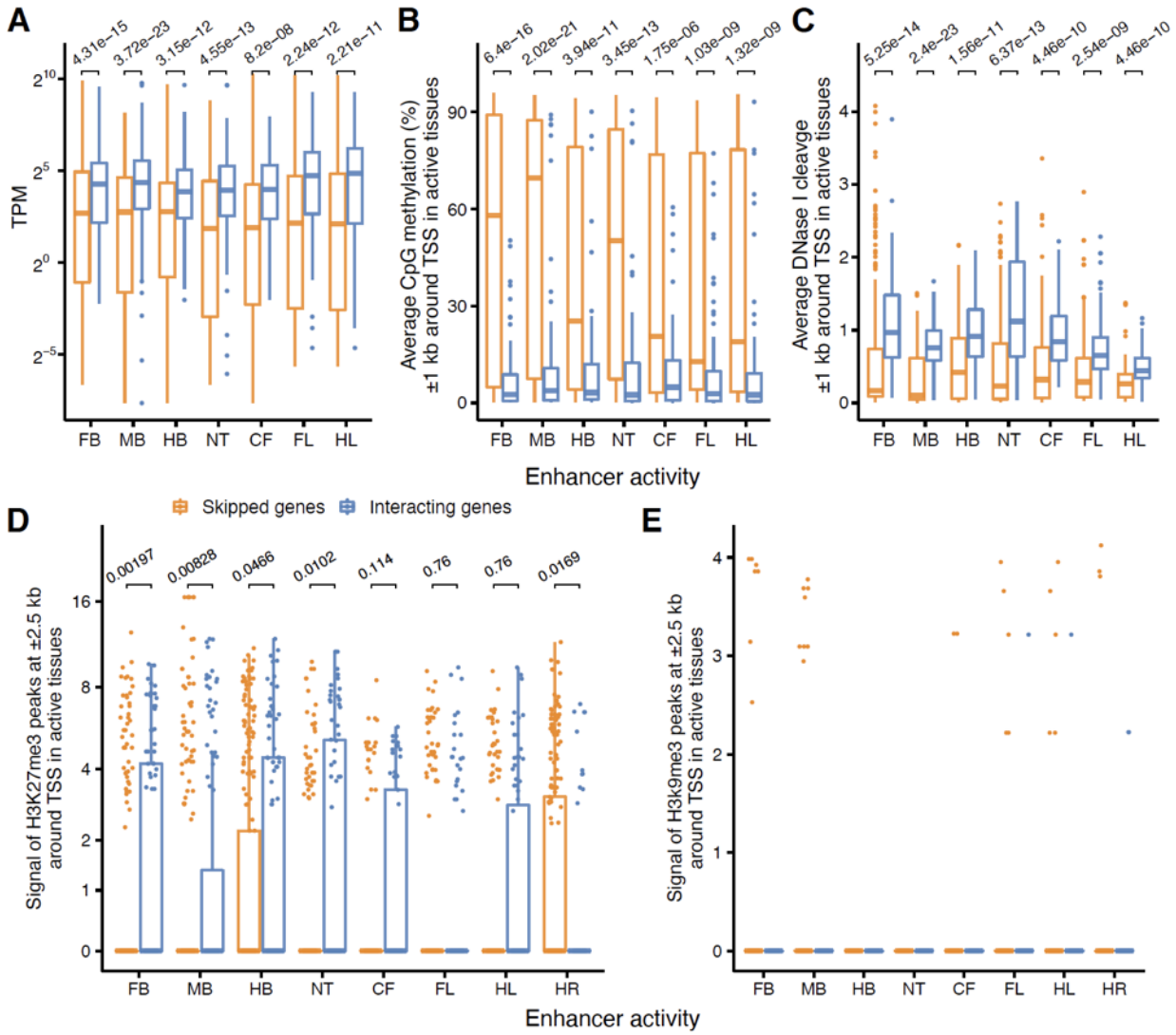

Supplementary Figure 3: Chromatin states of enhancer-interacting and enhancer-skipped promoters. Quantitation of mRNA expression levels (**A**), CpG methylation (**B**), DNase accessibility (**C**) at ±1kb, and H3K27me3 (**D**), H3K9me3 (**E**) signal at ±2.5 kb of enhancer-interacting and skipped promoters in tissues where enhancers are active. FB, forebrain. MB, midbrain. HB, hindbrain. CF, craniofacial mesenchyme. FL, forelimb. HL, hindlimb. NT, neural tube. HR, heart. *P* values were calculated by unpaired-sample two-sided Wilcox test and adjusted for multiple testing. A statistical test was not performed for H3K9me3 since most of the values are zero.

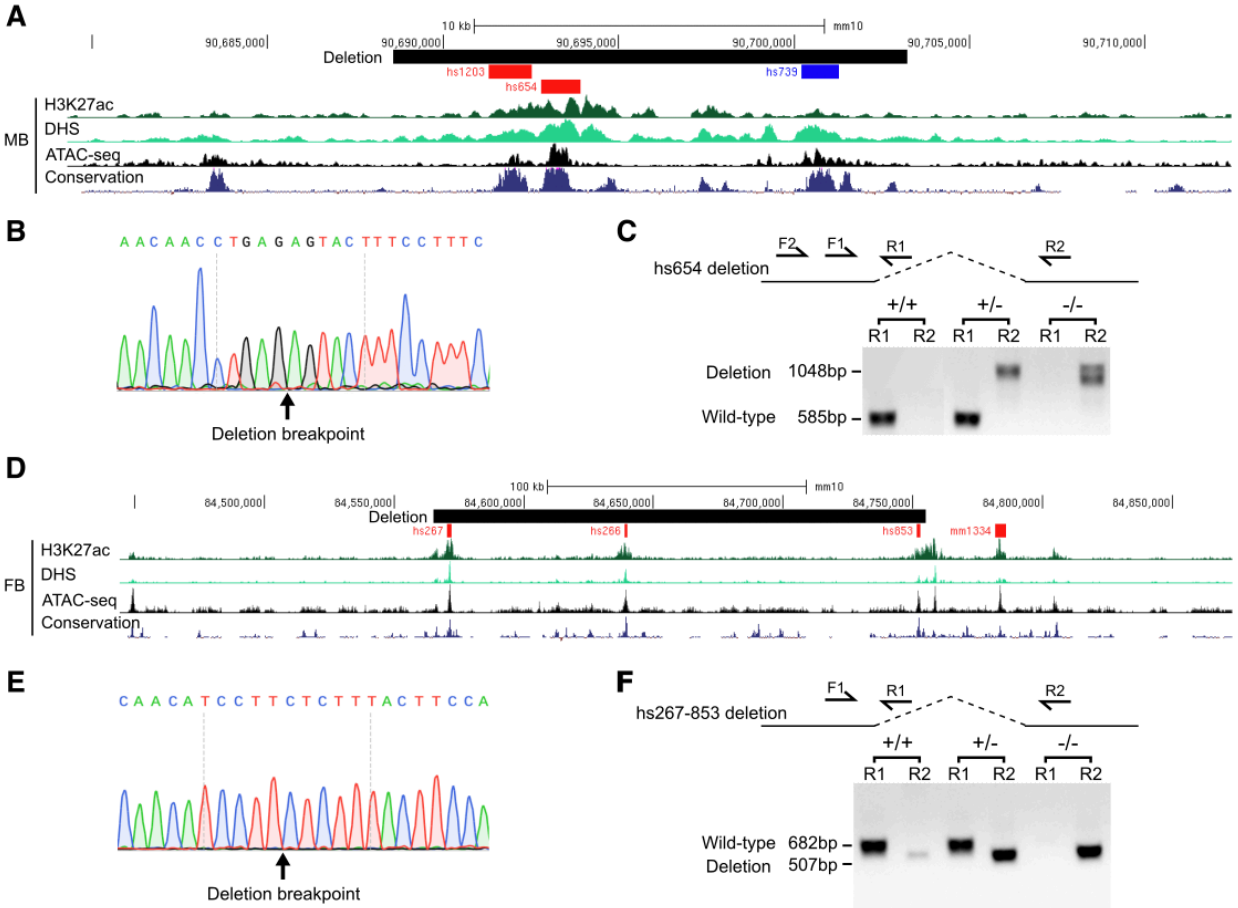

G

	Viability: Results from Heterozygous Female x Heterozygous Male Matings					
Enhancer	Pups Genotyped	+/+	+/-	-/-	chi-square	*P*-value
hs654	34	7	22	5	3.18	0.204
hs267-853	23	4	14	5	1.17	0.556

Supplementary Figure 4: CRISPR/Cas9-Mediated Enhancer Knockouts. (**A**) Schematic overview of H3K27ac, DNase-seq, ATAC-seq from midbrain and conservation track across 60 species of the deleted region encompassing hs654 enhancer from UCSC browser. (**B**) The PCR product from hs654-deletion mice was sequenced to identify deletion breakpoints. (**C**) PCR genotyping of the hs654 enhancer knockout mice. (**D**) Schematic overview of H3K27ac, DNase-seq, ATAC-seq from forebrain and conservation track across 60 species of the deleted region encompassing hs267, hs266 and hs853 enhancers from UCSC browser. (**E**) The PCR product from hs267-853-deletion mice was sequenced to identify deletion breakpoints. (**F**) PCR genotyping of the hs267-853 enhancer knockout mice. (**G**) Genotyping and Chi-Square test for viability of enhancer knock-out mice.

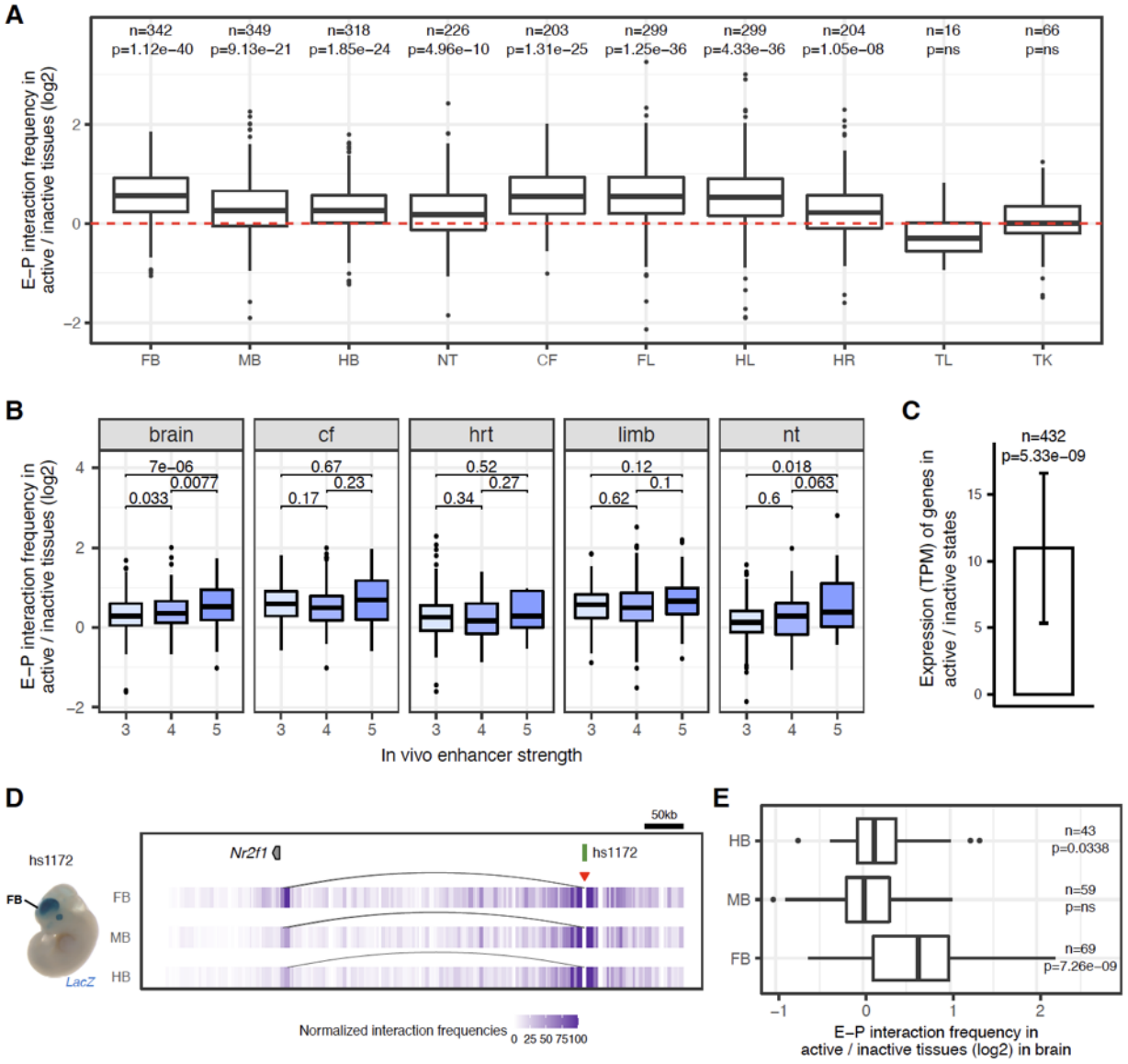

Supplementary Figure 5: E–P interaction frequency in active and inactive tissues. (**A**) The average ratio of enhancer-promoter interaction frequency between active and inactive tissues for enhancers active in individual tissues. The number of enhancer-promoter interactions and adjusted *P* values for each tissue are shown at the top. (**B**) The average ratio of enhancer-promoter interaction frequency between active and inactive tissues for brain enhancers with different strengths. Only tissues with more than 10 E–P interactions in each strength category were shown due to the number of invariant E–P interactions in those tissues is fewer than 20). (**C**) The fold-change of gene expression levels (TPM) between active state (baited enhancers interact with promoters in active tissues) and inactive state (baited enhancers don't interact with promoters or in inactive tissues). (**D**) Chromatin interaction profiles in forebrain, midbrain and hindbrain centered on the enhancer hs1172 in the *Nr2f1* locus (chr13:78,057,768-78,705,499; mm10). The *in vivo* activity of enhancer hs1172 is shown on the left. (**E**) The average ratio of enhancer-promoter interaction frequency between active and inactive tissues (only brain tissues) for enhancers only active in one of the brain domains (forebrain, midbrain or hindbrain). *P* values were calculated by paired-sample two-sided Wilcox test and adjusted for enhancers active in forebrain, midbrain and hindbrain.

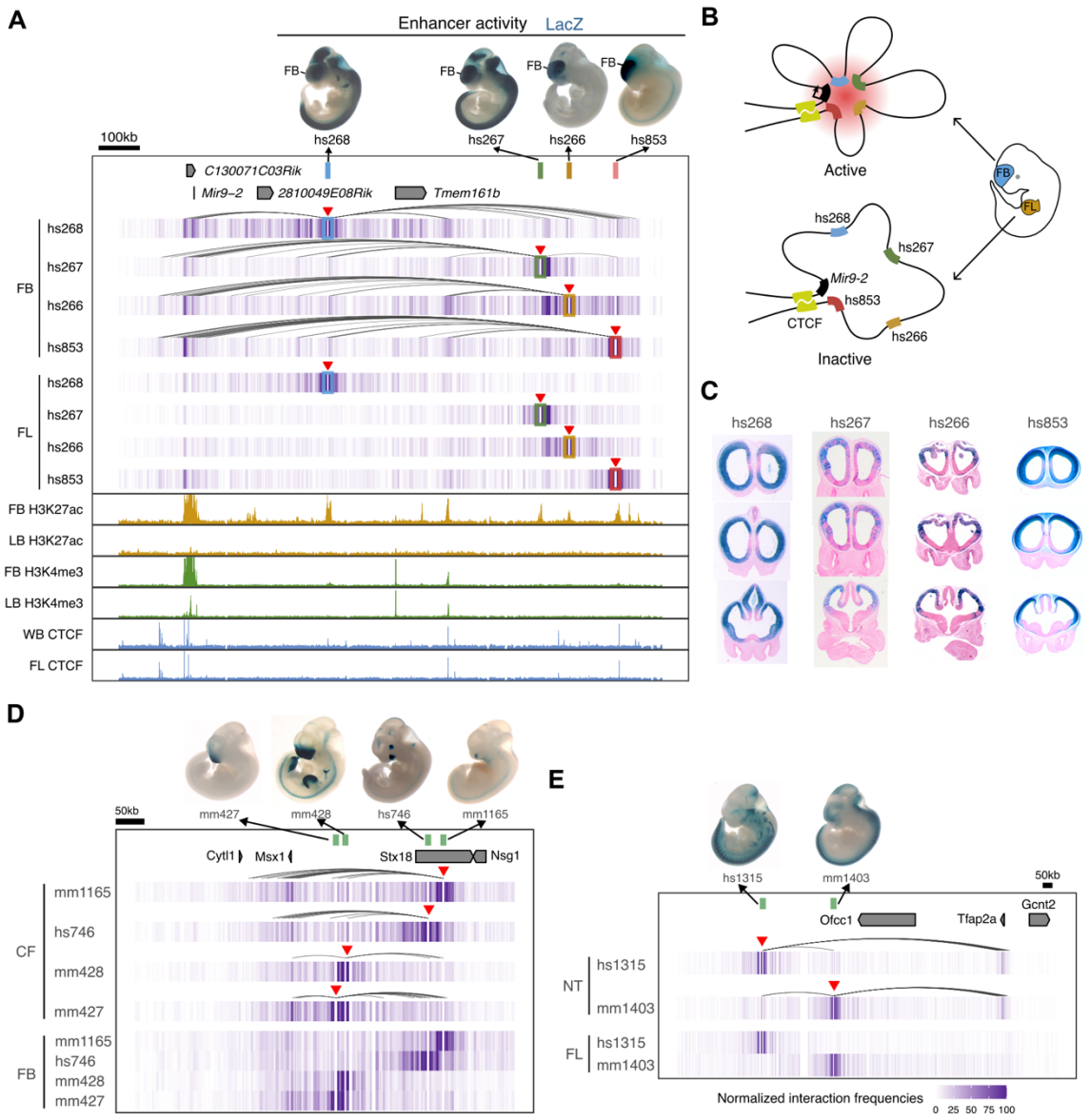

Supplementary Fig 6: Examples of enhancer—enhancer chromatin interactions. (**A**) The *Mir9-2* genomic region (chr13:83,558,457-84,861,438; mm10) is shown with chromatin interaction heatmaps centered on hs268 (blue), hs267 (green), hs266 (yellow) and hs853 (red) enhancers in the forebrain (FB) and forelimb (FL). The top left shows Mir9 in situ hybridization in E10.5 embryos. Shown on the top right are hs268, hs267, hs266 and hs853 enhancer activities in a transgenic mid-gestation (E11.5) mouse embryo. Red arrowheads indicate viewpoints. Arches indicate significant interactions in the forebrain. Shown on the bottom are H3K27ac (yellow) and H3K4me3 (green) ChIP-seq tracks in forebrain and limb buds (LB) at E11.5, CTCF (light blue) ChIP-seq tracks in the whole brain (WB) and forelimb at E12.5 (Gorkin et al. 2020; ENCODE Project Consortium 2012; Amândio et al. 2021; Rodríguez-Carballo et al. 2017). (**B**) Schematic depicting 3D chromatin interactions between enhancers and Mir9-2 gene in forebrain and forelimb. (**C**) Sections of in situ hybridization for gene C130071C03Rik and enhancer activity for hs268, hs267, hs266 and hs853 in E11.5 forebrain. (**D, E**) Chromatin interaction heatmaps centered on mm1165, hs746, mm428 and mm427 enhancers in the face (CF) and forebrain (FB) for Msx1 genomic region (chr5: 37,554,764-38,206,723; mm10) (D) and hs1315 and mm1403 enhancers in the neural tube (NT) and forelimb (FL) for Tfap2a genomic region (chr13: 39,098,000,41,000,000; mm10) (E). Shown on the top are mm1165, hs746, mm428, mm427, hs1315 and mm1403 enhancer activities in a transgenic mid-gestation (E11.5) mouse embryo. Arches indicate significant interactions.

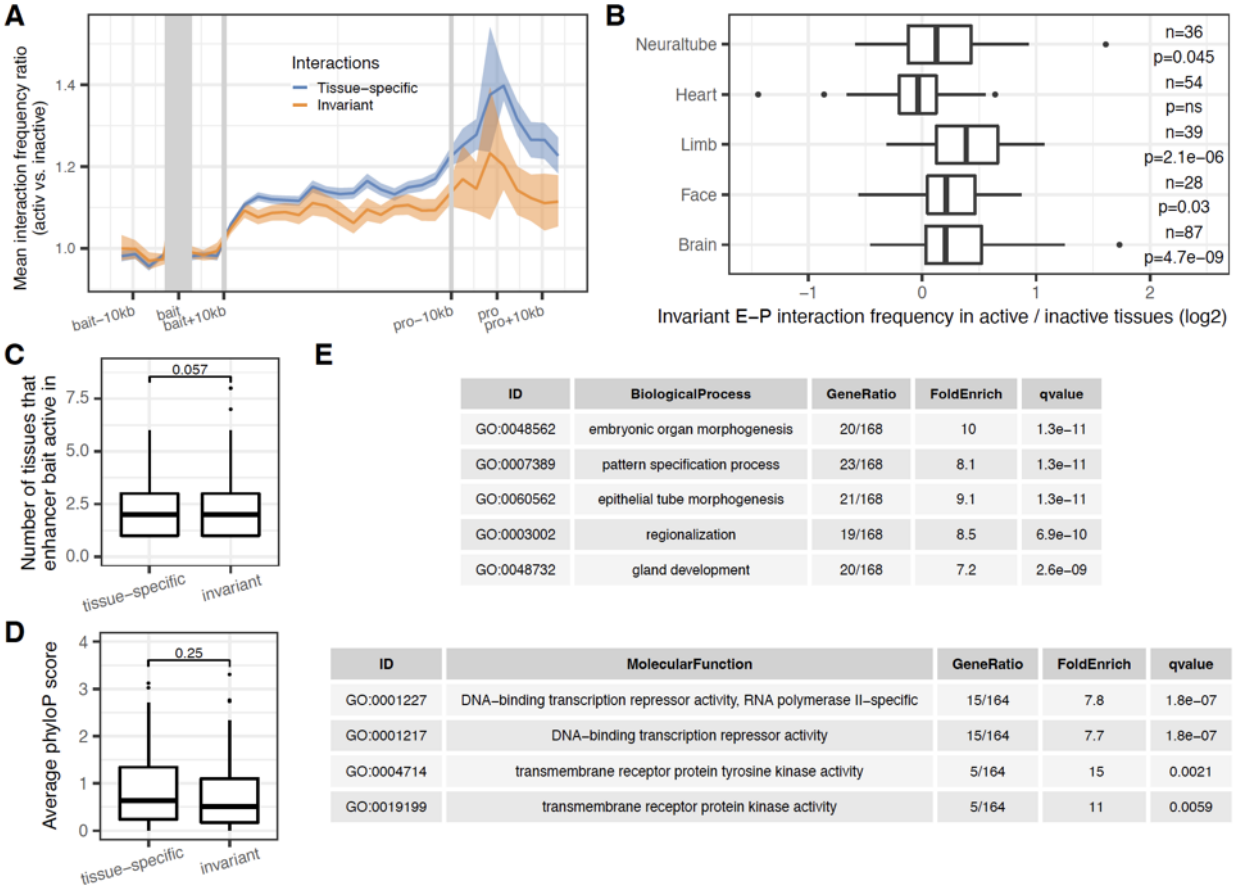

E

ID	BiologicalProcess	GeneRatio	FoldEnrich	qvalue
GO:0048562	embryonic organ morphogenesis	20/168	10	1.3e−11
GO:0007389	pattern specification process	23/168	8.1	1.3e−11
GO:0060562	epithelial tube morphogenesis	21/168	9.1	1.3e−11
GO:0003002	regionalization	19/168	8.5	6.9e−10
GO:0048732	gland development	20/168	7.2	2.6e−09

ID	MolecularFunction	GeneRatio	FoldEnrich	qvalue
GO:0001227	DNA−binding transcription repressor activity, RNA polymerase II−specific	15/164	7.8	1.8e−07
GO:0001217	DNA−binding transcription repressor activity	15/164	7.7	1.8e−07
GO:0004714	transmembrane receptor protein tyrosine kinase activity	5/164	15	0.0021
GO:0019199	transmembrane receptor protein kinase activity	5/164	11	0.0059

Supplementary Figure 7: Invariant E–P interaction frequency ratio between active and inactive tissues (**A**) Average ratio of enhancer-promoter interaction frequency between active and inactive tissues for tissue-specific ($n \leq 9$) and invariant ($n = 10$) interactions. Light blue shading indicates 95% confidence intervals estimated by non-parametric bootstrapping. (**B**) The average ratio of invariant enhancer-promoter interaction frequency between active and inactive tissues for enhancers active in the brain, face, limb, heart and neural tube E–P (data in other tissues are not shown due to fewer than 20 invariant E–P interactions in those tissues). *P* values were calculated by paired-sample two-sided Wilcox test and adjusted for multiple testing. (**C**) The number of tissues that enhancers in invariant ($n = 10$) or tissue-specific ($n \leq 4$) E–P interactions are active in vivo. (**D**) The average phyloP scores for enhancers in invariant ($n = 10$) or tissue-specific ($n \leq 4$) E–P interactions. P value shown above is calculated by Fisher's exact test. (**E**) GO enrichment for interacting genes in invariant E–P interactions (Biological process and Molecular function).

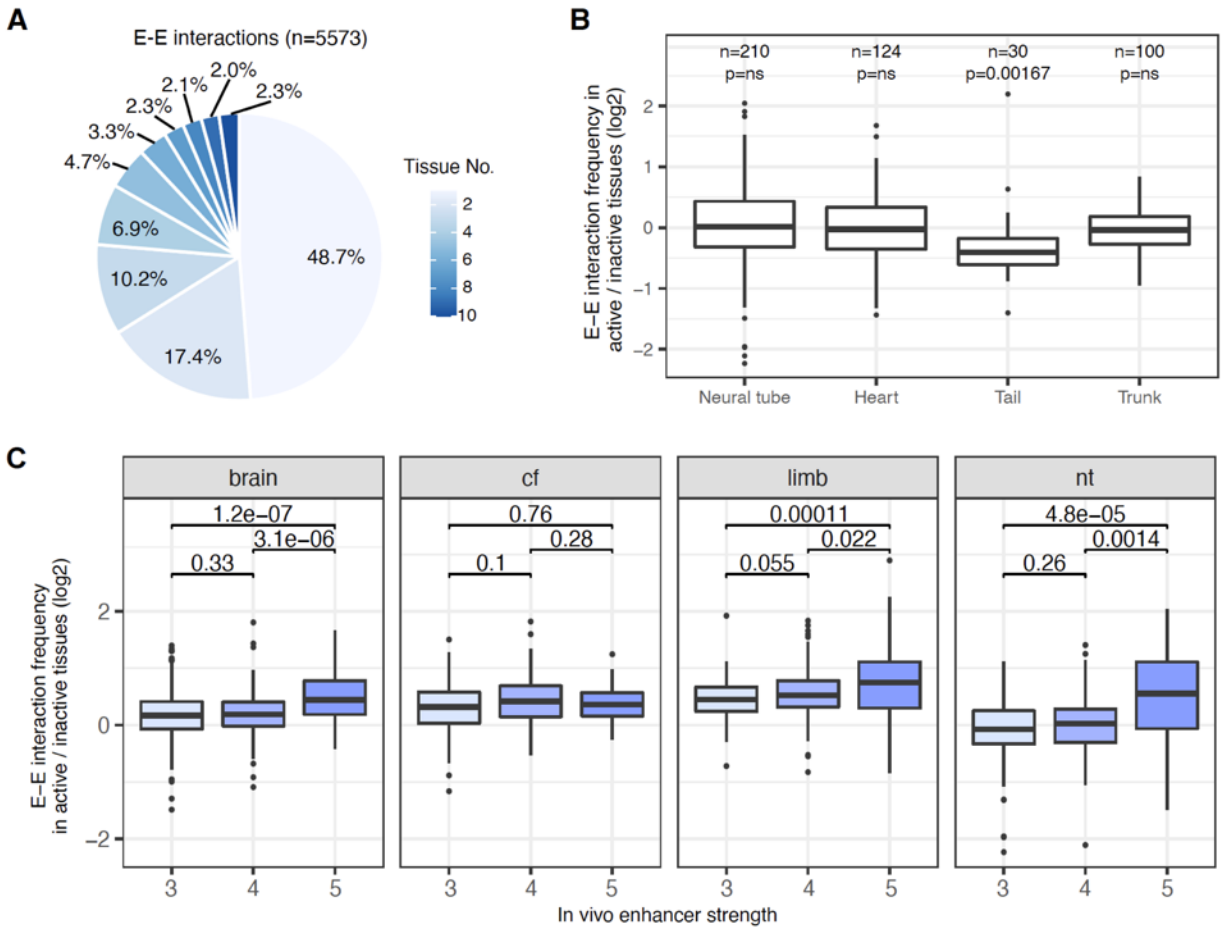

Supplementary Figure 8: Tissue specificity of enhancer-enhancer chromatin interactions (**A**) Pie chart showing the fraction of E–E interactions present in different numbers of tissues. (**B**) The average ratio of E–E interaction frequency between active and inactive tissues for enhancers active in neural tube, heart, tail and trunk. The number of E–E interactions for each tissue is indicated at the top. P values were calculated by paired-sample two-sided Wilcox test and adjusted for multiple testing. (**C**) The average ratio of enhancer–enhancer interaction frequency between active and inactive tissues for enhancers of different strengths in different tissues. Only include tissues with more than 10 E-E interactions in each strength category. P values were calculated by unpaired-sample two-sided Wilcox test with multiple testing.

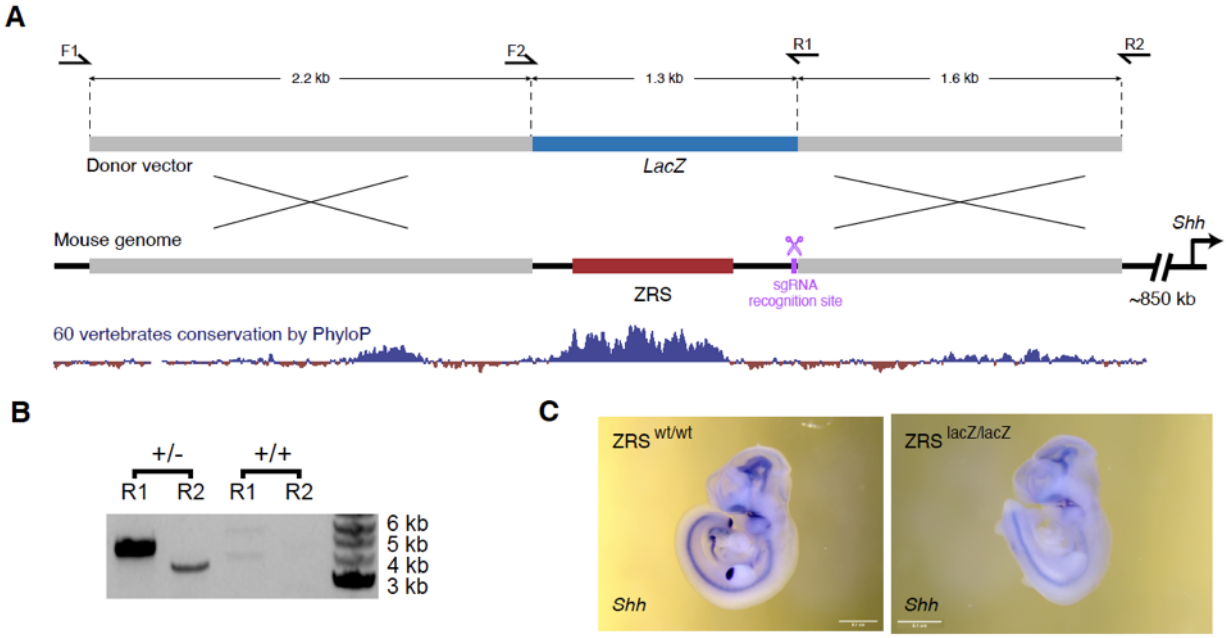

Supplementary Figure 9: CRISPR/Cas9-Mediated ZRS Limb Enhancer Replacement with LacZ by Homology-Driven Repair. (**A**) Schematic overview of the strategy for ZRS enhancer replacement. A 4.5 kb mouse genomic region containing the ZRS enhancer (red) is shown together with the vertebrate conservation track (dark blue). The donor vector contained two homology arms (gray) and a corresponding replaced region (blue) with borders. The sgRNA recognition site is indicated in purple. PCR primers used for genotyping are shown as arrows. (**B**) PCR genotyping analysis of heterozygous and wildtype mice using primer pairs LacZ-F1 and LacZ-R1 or LacZ-F2 and LacZ-R2. (**C**) Phenotypes of E10.5 ZRS wildtype and LacZ replacement mice embryos.

Supplementary Tables

Table S1.

Enhancer bait regions.

The first tab contains: mm10 coordinates of regions covered by Agilent RNA baits (1-3rd column), region name (4th column), type of the region (ENH for active enhancer, PRO for promoter and NEG for control elements, 5th column), Enhancer activity (6th column, only for ENH), number of RNA probes designed (7th column). The second tab contains the information for the number of unique di-tags mapped to the genome or bait regions for each replicate. The third tab contains the coordinates of regions covered by Agilent RNA baits in an ecHi-C experiment in Fig. 5G,H.

Table S2.

Enhancer-centric significant interactions.

The four separate tabs in Table S2 contain all significant enhancer-centric interactions with promoters (1st tab), CTCF sites (2nd tab), enhancers (3rd tab) and Polycomb regions (4th tab) in individual tissues. Each tab contains the following columns: mm10 coordinates of regions covered by Agilent RNA baits (1-3rd column), region name (4th column), type of the region (5th column), mm10 coordinates of the interacting fragment (6-8th column), corresponding CHiCAGO scores (9th column), tissue in which the interaction was called (10th column). The first tab also contains coordinates of interacting promoters (11th

column), gene names (12th column). The second tab also contains coordinates of interacting enhancers (11th column).

Table S3.

Interactions for regions linked to human congenital disorders

Table S3 contains the following columns: coordinates of regions encompassing mutations/variants in GRCh38 genome assembly (1-3rd column), mutation type (4th column), coordinates of overlapping enhancer regions (5-7th column), region name (8th column), enhancer activity (9th column), interacting gene (10th column), the phenotype of the patients harboring mutations/variants (11th column), reference or database for the mutations/variants (12th column).